Imperial/TP/3-04/15
hep-ph/0406202
18th June 2004

Testing an Optimised Expansion on Z_2 Lattice Models

T.S. Evans*, M. Ivin

Theoretical Physics, Blackett Laboratory, Imperial College London,
Prince Consort Road, London SW7 2AZ U.K.

arXiv:hep-ph/0406202v1 18 Jun 2004

Abstract

We test an optimised hopping parameter expansion on various Z_2 lattice scalar field models: the Ising model, a spin-one model and $\lambda\phi^4$. We do this by studying the critical indices for a variety of optimisation criteria, in a range of dimensions and with various trial actions. We work up to seventh order, thus going well beyond previous studies. We demonstrate how to use numerical methods to generate the high order diagrams and their corresponding expressions. These are then used to calculate results numerically and, in the case of the Ising model, we obtain some analytic results. We highlight problems with several optimisation schemes and show for the best scheme that the critical exponents are consistent with mean field results to at least 8 significant figures. We conclude that in its present form, such optimised lattice expansions do not seem to be capturing the non-perturbative infra-red physics near the critical points of scalar models.

1 Introduction

The aim of this paper is to study the LDE (Linear Delta Expansion), a non-perturbative method. Finding alternatives to weak-coupling perturbation expansions is vital as there are many problems where such methods fail even when the theory is weakly interacting, e.g. at phase transitions. Perhaps the most accurate non-perturbative method is lattice Monte Carlo, but this has trouble with fermions, non-zero charge densities and dynamical problems [1]. However, there are very few alternatives: large-N for continuum calculations is one example, a hopping parameter expansion on the lattice is another. Unfortunately, these non-perturbative methods can be poor e.g. see the expansions for critical exponents η and γ in three dimensions using large-N approximations in [2]. Thus it is important to develop alternative non-perturbative methods.

LDE is just such an alternative non-perturbative method. Basically, it is an optimisation of an existing standard expansion scheme. The earliest appearance of the term LDE we know is in [3, 4] and some of this emerged from the logarithmic Delta Expansion work of [5, 6, 7, 8]. However LDE is such a generic scheme that it has appeared in many contexts, has been rediscovered many times and under many names: Optimised Perturbation Theory [9, 10], Gaussian Effective Potential approximation [11], Variational Perturbation Theory [12, 13, 14, 15], Order Dependent Mapping [2], Screened Perturbation Theory [16], method of self-similar approximation [17], the variational cumulant

*E-mail: T.Evans@imperial.ac.uk, WWW: http://theory.ic.ac.uk/∼time/

expansion [18], action-variational approach [19]. The method has been applied to the evaluation of simple integrals [4, 20, 21, 22, 23], solving non-linear differential equations [24], quantum mechanics [4, 9, 11, 14, 22, 23, 25, 26, 27, 28] and to quantum field theory both in the continuum [9, 10, 12, 16, 22, 29, 30, 31, 32, 33, 34, 35] and on a lattice (discussed below).[1]

An important and recurring question is how good is LDE? It appears to be a quite arbitrary scheme though, as we will try to highlight in the next section, many of the supposed limitations of LDE are common to all other expansion methods. Likewise, widely accepted methods are not always as good as one might have supposed, see for example the large-N expansion of critical exponents in [2]. LDE has, in fact, been tested rigourously in QM where it has been shown to lead to fast convergence of calculations of "zero-dimensional" path integrals [20, 21] and of the anharmonic oscillator [14, 27, 28]. However, such rigour is probably unobtainable in QFT (see [23] for an interesting discussion), where in practice the only simple test is to compare results against physical results, or, failing that, Monte Carlo calculations.

One of our goals was to look at the accuracy of LDE calculations on the lattice, where we are in effect optimising hopping parameter expansions. The method can go beyond Monte Carlo results, e.g. one can easily handle finite charge densities [36], but here the idea is to focus on calculations where there are good Monte Carlo results, if not physical measurements, as these can then provide us with the 'true' answer against which to test our results. We chose to look at critical exponents in ϕ^4 field theories as these are computationally accessible, they have been studied extensively theoretically and they have physical relevance, as shown by the available experimental data for critical exponents [15].

Another goal was to extend the accuracy of existing LDE lattice studies. The literature on lattice LDE contains work on scalar theories [4, 18, 37, 38, 39, 40, 41, 42, 43, 44, 45, 46], pure gauge models [4, 19, 37, 38, 39, 40, 41, 42, 43] and gauged Higgs models [47, 48]. Where they have made comparisons with other techniques, the conclusions are usually positive. For instance (Jones strong coupling in gauge theory) or the comparison of gauge Higgs models near transition [47, 48]. However, as far as we know, all the work in the literature, except one pure gauge study [19], has worked only to third order in the expansion, doing the expansions by hand. To go to higher orders requires a computerised approach to the expansion. Thus our second aim is to investigate how this could be done.

The codes we developed were easily adapted for studies of both the full ϕ^4 QFT and spin models. Thus we will also look at the Ising and spin-1 models which fall into the same universality class as the full ϕ^4 model [2, 15, 49]. The feasibility of LDE for full field theories at higher orders will therefore be addressed while the numerical simplicity of the spin models can be exploited at various points. Specific results will be given for all three models.

In the next section we will outline the LDE in the context of our ϕ^4 field and spin theories on the lattice. Section three will examine our numerical results in detail, comparing these with our more limited analytical results in section four. The final section we summarise our conclusions.

[1]The wide applicability of this approach under different guises means our list in this paragraph is only a sample of LDE type papers, suitable as a starting point for further research. We do not claim to establish the precise history of the method. Also see [34] for comments about names.

2 The Free Energy Density in LDE

2.1 General Discussion of LDE

We will start by developing the LDE in very general terms by considering a theory described by the full action S which depends on physical parameters $\boldsymbol{p}$. We will be looking at scalar field theories where $\boldsymbol{p}$ will be masses and coupling constants.

It is helpful to focus on the calculation of a specific quantity, though the principles are the same for all quantities, so consider the partition function Z

$$Z(\boldsymbol{p}) := \mathrm{tr}\{e^{-S}\}. \tag{1}$$

The starting point for all expansions in QFT is that with the physical action for the theory of interest, $S = S(\boldsymbol{p})$, there is no exact solution[2] for Z. We therefore turn to some solvable theory described by an action $S_0 = S_0(\boldsymbol{v})$ which depends on a set of parameters $\boldsymbol{v}$. These parameters $\boldsymbol{v}$ of the solvable action S_0 will be specified later but for now we just note they may be different from the physical parameters $\boldsymbol{p}$ of the full action S. The idea is to expand about the trial action S_0, exploiting its solubility. To do this we replace the action S by S_δ the *δ-modified action*, i.e.

$$S(\boldsymbol{p}) \longrightarrow S_\delta(\boldsymbol{p},\boldsymbol{v}) = S_0(\boldsymbol{v}) - \delta\big(S_0(\boldsymbol{v}) - S(\boldsymbol{p})\big) \tag{2}$$

Then rather than considering the complete partition function Z of (1), we look at the *δ-modified partition function* Z_δ

$$Z(\boldsymbol{p}) = \mathrm{tr}\, e^{-S} \quad \longrightarrow \quad Z_\delta(\boldsymbol{p},\boldsymbol{v}) = \mathrm{tr}\{e^{-S_\delta(\boldsymbol{v})}\} = \mathrm{tr}\{e^{-S_0(\boldsymbol{v})}e^{-\delta(S_0(\boldsymbol{v})-S(\boldsymbol{p}))}\} \tag{3}$$

Clearly we need to set $\delta = 1$ at the end of the calculation to return to the appropriate action of the physical theory, $\lim_{\delta\to 1} Z_\delta = Z$. Thus the δ is *merely a book keeping parameter* introduced to keep track of the terms in the expansion about S_0

$$Z_\delta = \sum_{n=0}^{\infty} \frac{\delta^n}{n!} Z_n(\boldsymbol{p},\boldsymbol{v}) \tag{4a}$$

$$Z_n(\boldsymbol{p},\boldsymbol{v}) = \mathrm{tr}\left[e^{-S_0(\boldsymbol{v})}\left(S_0(\boldsymbol{v}) - S(\boldsymbol{p})\right)^n\right] \tag{4b}$$

where we have defined Z_n as the n^{th} order term in the expansion of Z_δ. The expansion is in terms of increasing powers of $S - S_0$ and the parameter δ is just a parameter of technical use that records the order in the expansion of any given term in the calculation. Note that without further information, demanding $|\delta| \ll 1$ is neither necessary nor sufficient to control the convergence of this series, so we need not be concerned that $\delta = 1$ is required at the end of the calculation.

Formally, summing all terms gives back the insoluble theory S when $\delta = 1$, but by assumption this can not be done here. However, we are free to choose S_0 so that individual terms in the expansion, Z_n, are obtainable, and in particular, the low order terms can be calculated in a reasonable amount of time. This is one major principle behind the choice of S_0. The idea is then to truncate the series, i.e. we consider

$$Z_\delta^{(R)} = \sum_{n=0}^{R} \frac{\delta^n}{n!} Z_n \tag{5}$$

[2] In some rare cases in QFT, we may be trying to construct an exact solution via some expansion, e.g. as in two-dimensional sine-Gordon models.

where the superscript of $Z_\delta^{(R)}$ denotes the order at which the expansion is truncated.

So far, all we have done is describe generic perturbation schemes. For later comparison, let us consider standard (weak-coupling) perturbation theory in this context. Then $S - S_0$ would be proportional to some small real coupling constant. For instance, in the ϕ^4 theories studied here we would choose $S - S_0 = -\int d^4x \lambda\phi^4$. Then we hope that for $0 \leq \lambda \ll 1$ the small parameter λ would ensure convergence, or at least that a truncated series gives good answers. In fact the former is clearly not true, QFT perturbation series do not usually converge, and the latter can also be false. The instability expected for λ negative, however small, indicates that physical results will not be analytic in the complex λ plane about $\lambda = 0$. Thus a series in λ can not be convergent. The behaviour of such series is hard to study in full QFT though it can still provide useful information by using ideas such as Borel summability.[3] However, whether the first few terms are a good approximation, despite these issues, changes depending on the question being asked of the model. For instance, while weak-coupling perturbation theory gives accurate results for QED, at phase transitions weak-coupling perturbation theory is known to break down even in weakly-interacting theories. Ultimately then, all expansions in QFT are developed using physical intuition that $(S-S_0)$ is suitably small, confirmed only by comparing with physical results. It is only posthoc, and usually only in a limited way (if at all), that a rigourous mathematical basis for the expansion can be given. QED is a successful example of this process, and it shows that despite the mathematical uncertainties, the procedure outlined so far is worth following. So here, as in all expansions in QFT, a second principle guiding the choice of S_0 should be that S_0 is chosen so that terms up to $n = R$ are sufficient to give a good approximation. Crudely speaking, $(S - S_0)$ is to be thought of as "small", while the size of the coefficient δ is one and does not control the convergence.

It is at this point that LDE departs from standard perturbative expansions, and where the non-perturbative aspects come in. In the LDE approach the parameters $\boldsymbol{v}$ of the trial action S_0 are fixed using a variational method. These *variational parameters* $\boldsymbol{v}$ lie at the heart of the LDE method and provide the mechanism through which non-perturbative behaviour is introduced into the model. Before the expansion is truncated, upon substitution of $\delta = 1$, the dependence on the variational parameters vanishes and we have the full theory which only depends on the physical parameters $\boldsymbol{p}$ in S, so $Z = Z(\boldsymbol{p})$. However, a truncated series $Z_\delta^{(R)}$, will have residual dependence on these unphysical variational parameters $\boldsymbol{v}$ even when $\delta = 1$, i.e. $Z_{\delta=1}^{(R)} = Z_{\delta=1}^{(R)}(\boldsymbol{p}, \boldsymbol{v})$. The final criteria for the choice of S_0 is that it has some variational parameters $\boldsymbol{v}$ suitable for our subsequent exploitation.

Clearly the dependence in the truncated answer on the arbitrary variational parameters $\boldsymbol{v}$ is unphysical. Thus the final stage of the LDE method is to fix the variational parameters. Most importantly, this is to be redone every time we repeat a calculation at a higher order. Thus the values we assign to the variational parameters depends on the order at which we truncate the expansion so we are expanding about *different* theories S_0 at each order. Thus this procedure has been called an order dependent mapping [2]. By contrast, if $\boldsymbol{v}$ was to be fixed at some specific order of the expansion and then used for all other orders, we would end up with nothing else than another perturbative expansion.

The aim is to fix the variational parameters to values which will produce a result

[3]Rigourous results for LDE are possible in one space-time dimension when the problem becomes one of the Quantum Mechanics of an anharmonic oscillator. See also [23] for a useful discussion of LDE and expansions in general.

closest to the true physical one. The problem in achieving this goal is that there is no unique prescription which tells us how to do this. We know of five broad categories of methods used to fix the variational parameters. PMS (the principle of minimal sensitivity) and FAC (fastest apparent convergence) are the two most common. The names PMS and FAC, and their systematic definitions were introduced in [9]. However, prior to this we find a PMS-like criterion used in a study of a variational Hartree-type expansion applied to ϕ^4 field theory [51] and used in QM [25, 26], and the FAC criterion used in [52] to calculate the energy levels of an anharmonic oscillator by a variational perturbative expansion. In continuum calculations, the use of gap equations (choosing variational parameters such that the self energy is zero and the full propagator has a pole at the variational mass) is a third approach. A fourth is that of Meurice [33] who cut off the range of integration of the fields.

However we shall focus largely on a fifth approach and fix our variational parameters by demanding that they minimise the free energy [18, 45]. This choice is simply based on the physical principle that the free energy density $f(\boldsymbol{p})$ of a system always tends to a minimum. Thus we seek a minimum of the function $f^{(R)}(\boldsymbol{p}, \boldsymbol{v})$ in the variational parameter phase space $\boldsymbol{v}$ whilst keeping the physical parameters $\boldsymbol{p}$ constant during the optimisation. This will fix the variational parameters to the optimum value, which we will denote with a bar as $\bar{\boldsymbol{v}}$ — a function of the physical parameters $\boldsymbol{p}$ and the order R. Likewise the optimum free energy density will then be

$$\bar{f}^{(R)}(\boldsymbol{p}) := f^{(R)}(\boldsymbol{p}, \bar{\boldsymbol{v}}) \leq f^{(R)}(\boldsymbol{p}, \boldsymbol{v}) \quad \forall\, \boldsymbol{v}, \tag{6}$$

for a given set of physical parameters $\boldsymbol{p}$. Assuming analyticity in $\boldsymbol{v}$ near $\bar{\boldsymbol{v}}$, we have

$$\frac{\partial}{\partial \boldsymbol{v}} f_\delta^{(R)} = 0 \tag{7}$$

At this optimal point $\boldsymbol{v} = \bar{\boldsymbol{v}}$, 'small' variations in the components of $\boldsymbol{v}$ produce 'negligible' variations in $f_\delta^{(R)}$, thus we are as close to being independent of the variational parameters as we will ever be. We will compare this minimum free energy principle against the other methods later in section 3.1.8.

2.2 Lattice scalar field models and LDE

Now let us apply this to specific models. We will consider theories of a single scalar field on a hyper-cubic Euclidean space-time lattice[4] with lattice spacing set to be 1 and of various dimensions with action

$$S = S_{\mathrm{UL}} + S_{\mathrm{NUL}} \tag{8}$$

$$S_{\mathrm{UL}} = \sum_{i \in \Lambda} J\phi_i + \alpha\phi_i^2 + g\phi_i^4 \tag{9}$$

$$S_{\mathrm{NUL}} = -\kappa \sum_{i \in \Lambda} \sum_{j \in \mathcal{N}_i^+} \phi_i \phi_j \tag{10}$$

We have split the action into two types of term. S_{UL} contains the ultra-local terms, involving products of fields from the same lattice point. The non ultra-local terms S_{NUL} have products of fields at different lattice points. The generic physical parameters $\boldsymbol{p}$ of the full action S are $\boldsymbol{p} = (\kappa, J, \alpha, g)$, though one can rescale the fields and remove any

[4]See conclusions in section 5 for comments on hyper-tetrahedral lattices.

one of these parameters. Λ is the set of space-time points, ϕ_i is the field value at site i, and $\mathcal{N}_i^+$ is the set of nearest neighbours to lattice point i in a positive direction.

For a full field theory we choose $\phi_i \in \mathbb{R}$ and exploit the freedom to rescale the field to set $\kappa = 1$ so the physical parameters are then $\boldsymbol{p}_{\rm qft} = (J, \alpha, g)$. To make contact with the the usual notation used for the spin-1 model, we set $g = 0$, use the rescaling freedom to choose $\alpha = 1$ so then $\boldsymbol{p}_{\rm spin1} = (\kappa, \alpha)$ and restrict ϕ_i to $\phi_i \in \{+1, 0, -1\}$. For Ising models we further restrict $\phi_i \in \{+1, -1\}$ but we still have $\boldsymbol{p}_{\rm ising} = (\kappa)$. All these models belong to the same universality class as the lattice ϕ^4 model [2, 15, 49].

The first step in LDE is to chose the trial action S_0 according to the three principles set out above, namely that S_0 describes a theory that we can solve, S_0 is a reasonable approximation to the full theory, and S_0 contains non-physical, variational parameters.

On a lattice, an action consisting of only ultra-local terms is soluble since the path integral factorises because the integral over the field at each space-time point is then independent of all the other field integrals. The insolubility of the full lattice ϕ^4 action (8) comes from the non-ultra-local terms $S_{\rm NUL}$ in the kinetic terms [1]. Thus we must choose a pure ultra-local action for our trial action S_0. Bearing in mind our second and third criteria for choosing a good S_0, a suitable guess for S_0 would be a trial action of the same form as the ultra-local part of the full action S but with arbitrary coefficients. Thus we introduce

$$S_0(\boldsymbol{v}) := \sum_{i \in \Lambda} L_0(\phi_i, \boldsymbol{v}), \tag{11}$$

where our trial action is ultra-local (solvable) and depends on the variational coefficients $\boldsymbol{v}$. One choice is to make this of the same form as the ultra-local terms of the full Lagrangian, (9), to be a close approximation to the full theory. So we will work with

$$L_0(\phi, \boldsymbol{v}) := \left[j\phi + k\phi^2 + l\phi^4 \right] \qquad \boldsymbol{v} := (j, k, l) \tag{12}$$

The variational parameters, j, k and l, are to be fixed by some optimisation condition once the expansion has been performed. In practice we do not always use the quartic variational parameter and in the Ising model both quadratic and quartic terms are trivial. In the end we will be left with expressions in terms of *statistical averages* $\left\langle \phi^p \right\rangle_0$ taken with respect to (11) where

$$\left\langle \phi^p \right\rangle_0(\boldsymbol{v}) := \frac{1}{\mathcal{Z}_0} \int \mathrm{d}\phi \, \phi^p \exp\{-S_0(\boldsymbol{v})\} = \frac{I_p}{I_0} \tag{13}$$

$$\mathcal{Z}_0(\boldsymbol{v}) := \int d\phi \, \exp\{-L_0(\phi, \boldsymbol{v})\} = I_0 \tag{14}$$

$$I_p(\boldsymbol{v}) := \int d\phi \, (\phi)^p \exp\{L_0(\phi, \boldsymbol{v})\}. \tag{15}$$

Note that the ultra-local property of L_0 is crucial and allows the factorisation into integrals over field values at a single site.

This is a good place to note that the expansions we are interested in are traditional lattice expansions, and it is the variational aspect which is novel. If we were to fix our variational parameters equal to the appropriate physical ones, i.e. $j = J$, $k = \alpha$ and $l = g$ in (11), then we would have an expansion in the the non-ultra-local term of S only. This is then a traditional strong coupling or *hopping parameter* expansion [1]. It is then not surprising that we can adapt the machinery developed for such traditional expansions [1, 53, 54, 55, 56, 57, 58] for the general LDE problem.

2.2.1 Trick for ultra local terms in $S - S_0$

If we recall the definition of the δ-modified action given in (2), we see that we have to expand $\exp\{\delta(S_0 - S)\}$ to a given order and evaluate the path integral with respect to the ultra-local $\exp\{S_0\}$. However, parts of $(S_0 - S)$ are also ultra-local and no more difficult to deal with than S_0. We can exploit this and make the diagrammatic evaluation below a great deal simpler. Thus let us make a further split of the action, replacing the physical action S by $S_{\delta\delta}$

$$\begin{aligned} S \longrightarrow S_{\delta\delta} &= S_1 - \delta_1 S_{\rm NUL}, & (16)\\ S_1 &:= S_0 + \delta_2(S_{\rm UL} - S_0) = \sum_{i\in\Lambda} L_1[\phi_i] & (17)\\ L_1[\phi_i] &:= (j + \delta_2(J - j))\phi_i + (k + \delta_2(\alpha - k))\phi_i^2 + (l + \delta_2(g - l))\phi_i^4 & (18) \end{aligned}$$

The idea is that we can do an expansion in δ_1 first up to the desired order R, treating $S_1 = S_0 - \delta_2(S_{\rm UL} - S_0)$ as an *intermediate variational action*. The parameter δ_2 then counts the powers of $-S_{\rm NUL}$ which contains all the non local terms in the calculation. As S_1 is ultra local, this expansion in δ_2 is just as feasible yet the diagrammatic methods used below are much simpler since there is only one type of term in $-S_{\rm NUL}$. This leaves us with an expression for a quantity of interest, such as Z, of the form

$$\begin{aligned} Z_{\delta 1}^{(R)} &= \sum_{n=0}^{R} \frac{\delta_2^n}{n!} Z_{1n} & (19)\\ Z_{1n}(\boldsymbol{v}, \delta_1) &= \mathrm{tr}\left\{ e^{-S_1(\boldsymbol{p},\boldsymbol{v},\delta_1)} \left(S_0(\boldsymbol{v}) - S(\boldsymbol{p})\right)^n \right\} & (20) \end{aligned}$$

We can see that to return to the proper LDE expansion of (2), we want to set $\delta = \delta_1 = \delta_2$ in (16) and truncate the series rigourously to order R in δ. Thus we have to do a further expansion to order $R - n$ in δ_1 of each term $Z_{1n}(\boldsymbol{v})$. In general this would be doubling the work we have to do to produce an overall δ expansion. However in this case we are expanding in powers of $(S_0 - S_{\rm UL})$ about S_0 and both are ultra local. This leads to this δ_1 expansion being significantly simpler than the first expansion in δ_2 and the non ultra local terms. We will see this means that there is no need to use the full diagrammatic machinery a second time. This will be clearer when we have finished outlining the complicated δ_2 expansion to which we now turn.

2.2.2 Partition function expansion

The expansions for all quantities can be expressed in terms of what we call *statistical averages* $\langle Q \rangle_1$, given in terms of our intermediate variational action (17):

$$\begin{aligned} \langle Q \rangle_1 &:= \frac{1}{Z_1} \int \mathcal{D}\phi \, Q \, e^{-S_1} & (21)\\ Z_1 &:= \int \mathcal{D}\phi \, e^{-S_1} & (22) \end{aligned}$$

For instance partition function can be written neatly as

$$Z_{\delta 1} = Z_1 \sum_{n=0}^{\infty} \frac{\delta_2^n}{n!} \langle (-S_{\rm NUL})^n \rangle_1. \quad (23)$$

It is useful to introduce a diagrammatic notation at this point and to use the language of graph theory (e.g. see [53, 59]). The whole space-time lattice is a *graph* whose

vertices are the space-time points. The edges of the lattice graph should be chosen to be those linking neighbouring space-time points which appear in non ultra-local products in the lattice action coming from the derivative terms. For our simple nearest neighbour approximation of the derivatives, the edges connect all nearest neighbour vertices. Thus each edge represents a unique nearest neighbour vertex pair and appears only once in the edge set of the lattice graph, i.e. our lattice graph is a *simple graph*. The non ultra local action can then be written as

$$-S_{\rm NUL} = \sum_{i\in\Lambda}\sum_{j\in\mathcal{N}_i^+} \overset{i}{\bullet}\!\!-\!\!\!-\!\!\overset{j}{\bullet} \tag{24}$$

$$\overset{i}{\bullet}\!\!-\!\!\!-\!\!\overset{j}{\bullet} := \kappa\phi_i\phi_j \tag{25}$$

From the diagrammatic point of view, performing the sum over i and j in $S_{\rm NUL}$ is equivalent to running over all the elements of the *edge set* of the lattice graph.

What this means is that the n-th order term in the δ_2 expansion of the partition function (22) is represented by a sum over all possible ways of choosing n edges from the edge set. We will call each choice a *configuration*. However note that we must include terms where we choose the same edge more than once. Thus in the language of graphs, our configurations include both simple and non-simple graphs. Only the simple configurations (i.e. ones which are simple graphs) are subgraphs of the lattice graph and these will be our main focus. We will see that the expressions represented by non-simple graphs represent straight forward generalisations of the expressions represented by some simple graph. We will use C to indicate a configuration of the lattice.

Statistical averages have one important property given that we have chosen our variational actions (S_1 here, S_0 ultimately) to be ultra-local, namely the statistical averages of any polynomial of fields is also factorisable into terms depending on fields at only one lattice point. First the normalisation in our statistical averages factorises

$$Z_1 = \int \mathcal{D}\phi\, e^{-S_1} = \prod_{i\in\Lambda}\int \mathrm{d}\phi_i \exp\left\{-L_1(\phi_i)\right\} = (\mathcal{Z}_1)^N, \tag{26}$$

$$\mathcal{Z}_1 := \int \mathrm{d}\phi \exp\left\{-L_1(\phi)\right\} \tag{27}$$

where L_1 is defined in (18). Note that for simplicity we are assuming here that the physical sources, $\boldsymbol{p}$, are space-time constants, so that we obtain the same normalisation factor $\mathcal{Z}_1$ whatever lattice site i is used in (22) (translational invariance).

We can now write our statistical averages as[5]

$$\left\langle (\phi_1)^{n_1}(\phi_2)^{n_2}\ldots(\phi_i)^{n_i}\ldots\ldots\right\rangle_1 = \frac{1}{Z_1}\int \mathcal{D}\phi\, e^{-S_1}(\phi_1)^{n_1}(\phi_2)^{n_2}\ldots(\phi_i)^{n_i}\ldots\ldots \tag{28}$$

$$= \left\langle(\phi_1)^{n_1}\right\rangle_1\left\langle(\phi_2)^{n_2}\right\rangle_1\ldots\left\langle(\phi_i)^{n_i}\right\rangle_1\ldots\ldots \tag{29}$$

$$= \frac{J_{n_1}}{J_0}\frac{J_{n_2}}{J_0}\ldots\frac{J_{n_i}}{J_0}\ldots\ldots \tag{30}$$

and they depend only on the integrals over fields at a single space-time point

$$J_n(\boldsymbol{v},\delta_1) := \int d\phi(\phi)^n e^{-L_1(\boldsymbol{v},\delta_1,\phi)} \tag{31}$$

[5]The statistical averages $\left\langle\phi^p\right\rangle_0$ defined in (13) with respect to L_0 of (11)have identical factorisation properties but now in terms of the I_p integrals of (15).

This gives us a simple translation from the statistical averages associated with configurations C to algebraic expressions:

$$\langle C \rangle_1 = \kappa^n \prod_{i \in C_{\text{vertex}}} \frac{J_{k_i}}{J_0} \tag{32}$$

where C_{vertex} is the set of vertices in configuration C. k_i is the connectivity of the i-th vertex, that is the number of edges in the configuration C which have one end at the i-th vertex. The configuration has n edges.

It is important to note that since we have translational invariance, the expressions depend only on the connectivities of a given configuration and not on the precise position of the configuration on the lattice. It is therefore useful to consider graphs which are not embedded on the space-time lattice, and these we call *diagrams*, D. Every diagram is isomorphic to many configurations yet all these configurations represent the same algebraic expression. The number of different ways we can embed the diagram in the space-time lattice, that is the number of configurations isomorphic to a diagram is called the *lattice constant* of the diagram. For instance the expression for the partition function is then

$$Z_{\delta 1} = Z_1 \sum_D (\kappa \delta_2)^n \frac{b_D}{n!} c_D \left(\prod_{i \in D_{\text{vertex}}} \frac{J_{k_i}}{J_0} \right) \tag{33}$$

Here the sum is over all possible graphs, simple and non-simple, connected and disconnected, as these are the set of diagrams D. The c_D is the lattice constant for the graph D while n is the number of edges in the diagram. The last factor, b_D, is a binomial factor coming from the fact that the same edge in a configuration of n edges, can come from any of the n factors of S_{NUL} in the $(-S_{\text{NUL}})^n$ terms. Allowing for non simple diagrams, we see that

$$\frac{b_D}{n!} = \prod_e \frac{1}{n_e!} \tag{34}$$

where the product is over all *distinct* edges, e, in the diagram, and n_e is the number of times each edge appears in the edge set of the diagram. Thus for any simple diagram, b_D is always $n!$, while for a maximally non-simple diagram, i.e. diagram of n identical edges, $b_D = 1$.

2.2.3 Free energy expansion

The partition function is not the easiest quantity to calculate. It involves all powers of the volume, here proportional to N the number of lattice sites. The free energy density, f, should be intensive and simpler to calculate. However, as the logarithm of the partition function it has a more complicated expression in terms of statistical averages so it is convenient to work with intermediate quantities called *cumulant averages* (also called *cumulant expectation values* or *semi-invariants*) and the expansion in terms of these averages is sometimes called a *cumulant expansion* or a *cluster expansion*[6]. We can

[6]The cumulant expansion owes its origins to studies in chemistry in the late 1930's. Starting in 1959, a series of papers [60, 61, 62] described the application of the expansion to the Ising model. Following papers [63, 64] further systematised the expansion, and applied it to the Ising and Heisenberg models. More recently, we find the cumulant expansion introduced and used in various ways and applied to a wide range of models. Some examples are [19, 44, 45, 18]. The approach we take to presenting the cumulant expansion is motivated by [53].

define the cumulant averages to play the same role for the free energy as the statistical ones did for the partition function [54]. Adapting to our case, where we are keeping $\delta_1(S_{\rm UL} - S_0)$ in the exponential and expanding initially just in powers of $-\delta_2 S_{\rm NUL}$ and truncating at order R we have by analogy with (23)

$$f := -\frac{1}{N}\ln(Z), \qquad f^{(R)} := \sum_{n=0}^{R} \frac{\delta_2^n}{n!} f_{1n} \tag{35}$$

$$f_{10} = -\frac{1}{N}\ln Z_1 = -\ln \mathcal{Z}_1, \qquad f_{1n} = -\frac{1}{N}\big\langle\, (-S_{\rm NUL})^n \,\big\rangle_{\rm C} \tag{36}$$

Note that we can use this to define the cumulant averages $\big\langle \dots \big\rangle_{\rm C}$.

These cumulant averages have several important properties which we will use to calculate them. First they are linear so that we can use the diagrammatic notation

$$\big\langle\, (-S_{\rm NUL})^n \,\big\rangle_{\rm C} = \sum_D b_D c_D \big\langle D \big\rangle_{\rm C} \tag{37}$$

where the sum is over all distinct order n diagrams, that is diagrams with n edges, and b_D and c_D are the binomial and lattice constant factors for diagram D exactly as we had above. Linearity together with the translation invariance in our model ($\boldsymbol{p}$ and $\boldsymbol{v}$ are space-time constants in our calculations) also means that every diagram is repeated once for each space-time point. Thus we can take advantage of this fact in future by calculating the embedding factors c_D of the graphs *per lattice site*, at the same time discarding the factor of $\frac{1}{N}$ sitting in front of the non-zero orders of the expansion in the above equation. However it is important to note that unlike lattice Monte Carlo calculations, our method works on a lattice of infinite size.

A second property is the systematic link between cumulant and statistical averages [19, 55, 56]:

$$\big\langle \Theta_{e_1} \cdots \Theta_{e_n} \big\rangle_{\rm C} = \sum_{\text{partitions of } (e_1 \dots e_n)} (-1)^{k-1}(k-1)! \underbrace{\big\langle \Theta_{e_1} \cdots \Theta_{e_r} \big\rangle_1 \cdots \big\langle \Theta_{e_s} \cdots \Theta_{e_n} \big\rangle_1}_{k \text{ factors}} \tag{38}$$

where Θ_e *must* always be one of the operators whose *sum* makes $S_{\rm NUL}$ in (37). Thus here it is an operator $\phi_i\phi_j$ associated with one edge $e = (i, j)$. It is vital to note that cumulant averages do *not* have a factorisation property analogous to that of the statistical expectation values (29).

Finally, we come to the crucially important *cluster property* of the cumulant averages. Given the ultralocal S_1 in the exponentials, the statistical averages in (38) factorise if *any* of the operators Θ_{e_i} does not depend on field values in any of the other Θ_e operators. One can quickly check that in this case the cumulant average vanishes. Put another way, the cumulant average of any disconnected graph is always equal to zero. A simple proof by induction can be found in [56], while the first general mathematical proof was presented in [65].

This last property is of great importance to us, because it vastly simplifies our task of calculating the $\big\langle\, (S_{\rm NUL})^n \,\big\rangle_{\rm C}$ terms.

If we put all of this together we arrive at a final formula

$$f^{(R)} \;:=\; \sum_{n=0}^{R} \frac{1}{n!} f_{1n} \tag{39}$$

$$f_{10} = -\frac{1}{N}\ln Z_1 = -\left[\ln \mathcal{Z}_1\right]_R, \qquad f_{1n} = -\sum_{D \in \mathcal{D}_c^n} b_D \frac{c_D}{N} \left[\big\langle D \big\rangle_{\rm C}\right]_{R-n} \tag{40}$$

The sum is over the set $\mathcal{D}_c^n$ of connected diagrams of n-links. The notation $[Q]_m$ indicates that we have to expand the quantity Q to order m in a δ_1 expansion

$$[Q]_m := \sum_{j=0}^{m} \frac{1}{j!} \left. \frac{\partial^j Q}{\partial(\delta_1)^j} \right|_{\delta_1=0} \tag{41}$$

A worked example is provided in appendix B.

2.2.4 Numerical evaluation of free energy

The first step is to find the lattice constants c_D. To do this we generate a complete set of *simple connected configurations* of up to R edges, modulo translation invariance. The algorithm used was inspired by one used in percolation theory [66, 67] and is outlined in appendix A.

We then have to see which of these configurations are isomorphic to a given diagram diagram D so that we can obtain the lattice embedding constant c_D for each diagram. To do this we use a *canonical labelling* for our configurations, that is for each configuration we map it to an abstract graph that has a unique labelling. In this way we know that if and only if two configurations are assigned to the same abstract graph are they identical. To do this we used a small part of McKay's beautiful set of graph routines called *nauty*[7] [68].

It is a simple matter of combinatorics to generate the b_D and c_D/N for all the non-simple but connected diagrams D up to order R by duplicating existing links in lower order simple diagrams.[8]

Thus this stage of our computation provided a list of all connected diagrams up to order R, together with their $b_D c_D/N$ coefficients for a specific lattice and in specific number of dimensions. However, the list can be used for any model where the only non-ultra local term is a nearest neighbour interaction. Our compiled programme producing this list of diagrams was relatively fast on, and used little memory of, a common desktop computer, typically taking less than a day.

The next stages were implemented using the interpreted algebraic manipulation programme, MAPLE [69]. This performed the transformation of the cumulant averages represented by the diagrams calculated previously $\left\langle D \right\rangle_{\rm C}$, into the expressions in terms of statistical averages, $\left\langle \ldots \right\rangle_1$. It then had to expand each statistical average in terms of δ_1. This involves replacing each J_p integral of (31) with the appropriate expression in terms of I_p integrals of (15) using the L_0 defined in (12). Moving from J_p to I_p integrals requires explicit knowledge of the ultra-local terms in both the action and the variational action and so is highly model dependent. The complete expression for each diagram D is then truncated to order R in $\delta = \delta_1 = \delta_2$. Putting the expressions for each diagram together with their coefficients gives an expression for the free energy. MAPLE then outputs optimised C language routines for the free energy expressions. Thus each run providing a routine for a specific model in a specific number of dimensions and on a specific type of lattice. Results were checked by taking appropriate limits (easy in MAPLE) of code for the third order expressions produced independently in an earlier study [45].

The advantages of using MAPLE were that development is relatively easy, it is extremely easy to alter the code to suit different models or to produce code for derivatives

[7] The name arises by forming an acronym from *No AUTomorphisms, Yes?*.

[8] In our implementation, some of our non-simple diagrams were isomorphic to others in our list but this redundancy is relatively small.

of the free energy, and it produces fast C routines for the final stage of our analysis. The disadvantage is that as interpreted code it is relatively slow. Never the less, using only basic optimisations, the MAPLE code for seventh-order ran just within the memory (1Gb) and speed (one day) limitations of a desktop computer. It is clear that to go to higher orders a compiled version of these algorithms would have to be used. The main job of the MAPLE code is to produce and manipulate truncated polynomials with a relatively limited types of coefficient. Thus writing explicit compiled code for this part is feasible.

The third and final stage of our numerical evaluation was implemented as another compiled programme. Using the free energy routines provided by the MAPLE programme, the task was to find a set of values for the variational parameters $\boldsymbol{v}$ which minimised the free energy for a given set of physical parameters $\boldsymbol{p}$. The I_p integrals required (for the full field theory case) are relatively straightforward to integrate, essentially dominated by a single peak in the integrand, so standard routines of [70] are sufficient. Our experience also showed that standard techniques to find the minimum in the multi-dimensional variational parameter space [70], that defined by $\boldsymbol{v}$, were successful. The practical problems encountered lay elsewhere.

The first problem is that the expressions for the full seventh order free energy are enormous. The files for the free energy $f^{(R)}$ grew as follows: $R = 1$ used 6Kb, $R = 3$ used 40Kb, order $R = 5$ used 0.5Gb and for $R = 7$ we had a 5Gb file. We found we needed about $1.5Gb$ of memory to compile our seventh order routines. A rough guess for the size of the 9th order code file would be approximately 50 gigabytes in size, beyond the limits of desktop computing.

However, this size indicates part of another serious problem, namely numerical accuracy. Our 7th order code is a sum of a vast number of terms, each term being a product of several variational and physical parameters, some very large integer constants $b_D c_d/N$, and several I_p integrals. Each of the I_p integrals must in turn be evaluated numerically involving many additions. Worse near a critical point where typically $j \to 0$ there is a large variation in the size of the terms. Some, such as I_p for p odd, approaching zero as $j \to 0$. Further, we are interested in variations of the free energy as its parameters are altered by small amounts. For instance, to locate the minima in variational parameter space, we will often need to compare $f^{(R)}(j = 0)$ against $f^{(R)}(j = \epsilon)$ for small ϵ. Variations in the physical parameters are used to calculate physical quantities such as $\langle\phi\rangle$. Thus tiny terms in the expressions for the free energy may well be significant for the overall change in the free energy. Just as bad, it is important to ensure that the variations in large terms, which may be only small fractions of the total value of that term, are also accurately calculated. A careful study of even the third order calculations suggests that the double precision accuracy available on typical `C++` compilers for desktop PCs may not be sufficient. Thus we implemented our codes using arbitrary precision arithmetic, provided by the GNU multiple precision routines [71]. This enabled us to choose the accuracy of all our computations at the start of a run. For instance we were able to use 256 bit arithmetic providing about 70 decimal places of accuracy. Further details and examples are provided in appendices C and D.

2.3 Physical Quantities

The free energy is not the only quantity of interest. We can also calculate various derivatives of the free energy and it is the behaviour of these at the critical point which are directly linked to critical exponents.

Let us use the example of $\langle\phi\rangle$ to illustrate issues which apply to all our calculations of derivatives of the free energy. Not only is this quantity the order parameter for the expected phase transition, but it is also the quantity which will give us an estimate of the critical exponent β (see equation (57)). Analytically, $\langle\phi\rangle$ is related to the free energy through

$$\langle\phi\rangle = \frac{\partial f}{\partial J} \tag{42}$$

However, we are not dealing with the full free energy density, but rather with the truncated version $f^{(R)}$. For this reason, we shall take a closer look at how we can make use of the above equation to calculate the field expectation value.

One way of proceeding is to use the values of our optimised free energy $\bar{f}^{(R)}(\boldsymbol{p}) := f^{(R)}(\boldsymbol{p}, \bar{\boldsymbol{v}})$ directly to numerically estimate $\langle\phi\rangle$. After all, once we have optimised $f^{(R)}$, we do have our best guess for the free energy and that is meant to contain all the thermodynamic information. The idea is straightforward to implement using

$$\langle\bar{\phi}\rangle^{(R)}_{\text{diff}} \approx \frac{\bar{f}^{(R)}(J+\epsilon) - \bar{f}^{(R)}(J)}{\epsilon} \tag{43}$$

This way, we have to make two optimisations of $f^{(R)}$: once using some value J for the physical source, and another time using $J+\epsilon$, where ϵ is some very small number. Note that this involves taking the difference of two free energies which may be very similar in size and we are only able to do this because we can choose whatever accuracy we require for our numerical calculations.

The alternative approach is to produce explicit code for $\langle\phi\rangle^{(R)}(\boldsymbol{p}, \boldsymbol{v})$ and to set the variational parameters, $\bar{\boldsymbol{v}} = \bar{\boldsymbol{v}}(\boldsymbol{p})$ to give a result

$$\langle\bar{\phi}\rangle^{(R)}_{\text{expl}}(\boldsymbol{p}) = \langle\bar{\phi}\rangle^{(R)}_{\text{expl}}(\boldsymbol{p}, \bar{\boldsymbol{v}}). \tag{44}$$

The subscripts on the $\bar{\phi}^{(R)}$ indicate where the result was obtained via differentiation of optimised free energies (diff) or via substitution of values of $\boldsymbol{v}$ which optimise the free free energy into the explicit expressions for $\bar{\phi}^{(R)}$ (expl). This is straightforward in principle as it is relatively trivial to implement the derivatives required by (42) in MAPLE on the general algebraic expressions, and then it can produce optimised `C` routines for the final numerical evaluation, just as we did for the free energy.

The difference is with $\bar{\phi}^{(R)}_{\text{diff}}$ we must produce optimised variational parameters $\bar{\boldsymbol{v}}(\boldsymbol{p})$, functions of the physical parameters $\boldsymbol{p}$, at two physical values, $J+\epsilon$ and J while for $\bar{\phi}^{(R)}_{\text{exp}}$ we only optimise the free energy at J (other physical parameters held constant).

However, it is not quite so simple and it is instructive to have a more detailed look at this explicit code approach to the physical quantities. From equation (42) we see that

$$\langle\phi\rangle = \frac{\partial f}{\partial J} = -\frac{1}{N}\frac{1}{Z}\frac{\partial Z}{\partial J} \tag{45}$$

where the generating function Z is of the form

$$Z = \text{tr } e^{-S_0(j,k,l)} e^{\delta\Delta S(J,\alpha,g;j,k,l)} \tag{46}$$

with $\Delta S = S_0 - S$. The second exponential in the above equation is the one that is expanded and truncated at some order R. Also in this term is the ΔS term that carries all the J dependence. Thus, by using equation (45) as a basis for calculating $\langle\phi\rangle$, i.e. differentiating f by the physical source J, we would bring down a power of δ as well as a

factor of ϕ. If this was done on expressions for f^R, then we would actually be producing an expression for $\delta\langle\phi\rangle$ which has only $(R-1)$ terms in the delta expansion, and we have $\langle\phi\rangle$ only up to $O(\delta^{R-1})$. Put another way, the lowest order term in $f^{(R)}$ is $\ln(Z_0)$ which is independent of physical parameters like J and this the term lost.

One solution is to develop a new diagrammatic expansion for $\langle\phi\rangle$ but this is costly and unnecessary. The solution to this loss of one order is to note that the first exponential contains S_0 with a term linear in ϕ yet no factor of δ. So if we were to differentiate with respect to the variational source j instead of the physical source J, we bring down a sole factor of ϕ. The problem is, of course, that S_0 in ΔS carries j dependence too, so direct differentiation by the variational source would be of no use as it would produce other terms. Yet, all is not lost, because we can still use a trick to extract a factor of ϕ from S_0 without interacting with the ΔS terms.

We notice that the j coming from the e^{-S_0} term in the partition function is actually never seen explicitly in the full development of the free energy density — it is always hidden in the I_p integrals. On the other hand, the j coming from the $e^{\delta\Delta S}$ term appear only in factors of

$$\Delta J := J - j \tag{47}$$

which are polynomial coefficients in the δ_1 expansion of the J_p integrals. It is easy then to keep δJ constant while taking a partial differential with the remaining j factors by in effect only differentiating the I_p factors with respect to j

$$\frac{\partial I_p(j,\Delta J)}{\partial j} \quad = \quad -I_{p+1} \tag{48}$$

To perform the $\frac{\partial f^{(R)}}{\partial j}$ operation, we can go through the explicit expression of each f_n (c.f. equation (92)) and replace every occurrence of I_p by the right hand side of equation (48). It is straightforward to do the necessary replacements of the I_p in MAPLE and it produces optimised `C` code for $\langle\phi\rangle^{(R)}(\boldsymbol{p},\boldsymbol{v})$. Finally, for particular physical values $\boldsymbol{p}$ we can substitute the appropriate variational parameters $\bar{\boldsymbol{v}}$, which were determined by the relevant optimisation condition (minimising free energy, PMS, FAC etc.). Thus we can obtain $\bar{\langle\phi\rangle}^{(R)}_{\text{expl}}(\boldsymbol{p}) = \langle\phi\rangle^{(R)}_{\text{expl}}(\boldsymbol{p},\bar{\boldsymbol{v}})$.

Another physical quantity of interest is the susceptibility χ. It is defined by

$$\chi = -\frac{\partial^2 f}{\partial J^2} \tag{49}$$

and is estimated in much the same way as $\langle\phi\rangle$ above. That is to say, we will use both the direct numerical approach, and the approach in which the individual orders of $\chi^{(R)}$ are explicitly obtained. The direct numerical approach makes use of:

$$\bar{\chi}^{(R)}_{\text{diff}} = \frac{\bar{f}^{(R)}(J+\epsilon) - 2\bar{f}^{(R)}(J) + \bar{f}^{(R)}(J-\epsilon)}{\epsilon^2} \tag{50}$$

Alternatively, finding the explicit cumulant expansion of χ proceeds by applying the recipe we introduced for calculating $\langle\phi\rangle$:

$$\chi^{(R)} = \frac{\partial^2 f^{(R)}(j,\Delta J)}{\partial j^2} \tag{51}$$

with ΔJ defined in (47). Writing $\chi^{(R)}$ as an expansion, we identify the individual orders:

$$\chi^{(R)}_{\rm expl}(\boldsymbol{p};\boldsymbol{v}) = \sum_{n=0}^{R} \frac{\delta^n}{n!}\chi_n \quad \Longrightarrow \quad \chi_n = \frac{\partial^2 f_n(j,\Delta J)}{\partial j^2} \tag{52}$$

As for the calculation of $\langle\phi\rangle$, we employ Maple to form optimised routines for $\chi^{(R)}_{\rm expl}(\boldsymbol{p};\boldsymbol{v})$. The optimum value $\bar{\chi}^{(R)}$ is given by substituting the appropriate set of physical parameters and the values for the variational parameters obtained by optimising the free energy

$$\bar{\chi}^{(R)}_{\rm expl}(\boldsymbol{p}) := \chi^{(R)}_{\rm expl}(\boldsymbol{p};\bar{\boldsymbol{v}}). \tag{53}$$

To summarise, we have identified two different approaches for evaluating some physical quantity Q (once the free energy density $f^{(R)}$ has been used to fix the variational parameters). We can estimate Q directly using the optimised free energy density $\bar{f}^{(R)}(\boldsymbol{p})$, taking differentials of this function. Variational parameters lose significance once they have been used to optimise $f^{(R)}$ (c.f. equation (43)). Alternatively we produce an explicit expansion for $Q^{(R)}(\boldsymbol{p};\boldsymbol{v})$. Some scheme is then needed to produce the optimised values of the variational parameters $\bar{\boldsymbol{v}}$, which could be derived either from the $Q^{(R)}(\boldsymbol{p};\boldsymbol{v})$ expression itself in which case the optimised values vary with the quantity Q of interest. Alternatively the values which optimise the equivalent free energy expression might be used. However the optimised values $\bar{\boldsymbol{v}}$ are obtained, they are used to give the estimated result for Q, $\bar{Q}^{(R)}(\boldsymbol{p}) := Q^{(R)}(\boldsymbol{p};\bar{\boldsymbol{v}})$. One of our aims will be to produce results using both methods and to compare them.

3 Results

3.1 Ising Model

We will start our discussion of results by looking at the Ising model since this model reproduces most of the behaviour spin-1 model and of the full ϕ^4 model with the benefit of being numerically less complex. This numerical simplification comes from two aspects: the restricted degrees of freedom, $\phi_i = \pm 1$, and the reduced number of variational parameters, $\boldsymbol{v} = (j)$. The trial action is defined with only one variational parameter because ultra-local quadratic and quartic terms are constant in the Ising model. The definition of S for the Ising model (8) leaves the model depending on two physical parameters $\boldsymbol{p} = (\kappa, J)$. We will refer to κ as the *inverse temperature*[9].

The restriction of the field to ± 1 reduces the I_p factors to simple functions

$$I_p = \begin{cases} 2\cosh(j) & \text{p even} \\ -2\sinh(j) & \text{p odd} \end{cases} \tag{54}$$

3.1.1 Fixing the Variational Parameter

Let us first consider the case with no physical source J. Then, as in [45], we find that the linear variational parameter, j, provides allows symmetry breaking to occur in this lattice LDE approximation. As long as $J = j = 0$, the trial action is invariant under the transformation of $\phi_i \to -\phi_i$. Once $j \neq 0$, the symmetry no longer holds, unless it

[9] In the literature, the symbol β is predominantly used to denote the inverse temperature of an Ising model. We use κ to avoid a notation clash with the critical exponent β.

is accompanied by the transformation $j \to -j$. For instance the free energy for fixed physical parameters $\boldsymbol{p} = (\kappa, J = 0)$ is an even function of j. Thus $j = 0$ is guaranteed to be a turning point in variational space for $J = 0$ problems. This behaviour is illustrated in figure 1, which shows plots of $f^{(7)}(\kappa, J = 0; j)$ vs. j for various values of κ. The

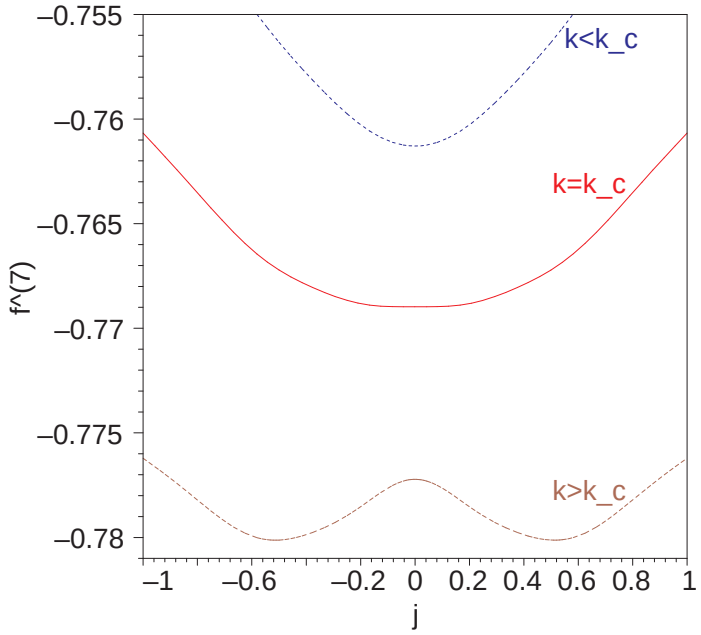

Figure 1: Plot of $f^{(7)}(\kappa, J = 0; j)$ vs. j for three different values. These are $\kappa = \kappa_c - 10^{-2}$, $\kappa = \kappa_c$, and $\kappa = \kappa_c + 10^{-2}$. The free energy is of the 3D Ising model at 7th order.

turning point at $j = 0$ need not be the unique minimum but what we find is that the free energy profile has a simple form as a function of j. It is straightforward to apply our principle of lowest free energy to choose the optimal variational parameter value $\bar{j}$. When $\kappa < \kappa_c$, the function $f^{(7)}$ indeed has a unique minimum at $j = 0$. For $\kappa \to \kappa_c$, we find the region around $j = 0$ flattening, and finally for $\kappa > \kappa_c$ the free energy displays two clear minima, either side of $j = 0$ with the $j = 0$ becoming a maximum. Both these minima are equally valid optimum points for j as guaranteed by the Z_2 symmetry of the model ($J = 0$). Numerically, the simplex optimisation method will choose one of the two minima, depending on the initial step of the routine.

We can already make several deductions. The optimal value $\bar{j}$ is a continuous but not smooth function of κ. This behaviour immediately tells us that our optimal value for the free energy will not be a smooth function of the physical variable κ. Thus we clearly see that there will be some sort of phase transition at κ_c and the variational source is itself a good order parameter even though it is not a physical observable.

Also note that for the Ising model we find good global free energy minima for both odd and even orders. We will comment further on this later.

3.1.2 Non-zero Physical Source

For various calculations, we will require the behaviour of the optimised free energy as a function of the physical source J in the region of $J = 0$. Turning on the physical source, we break the Z_2 symmetry and 'skew' the free energy vs. j curves. In the broken phase, one of the two minima acquires a lower free energy than the other, depending on the sign of the source. This effect can be seen in figure 2, where we plot the free energy curves

with the system in the broken phase. The inverse temperature is $\kappa = \kappa_c + 0.03$, and we use three different values for the physical source. These are $J = 0$, $J = 0.002$ and

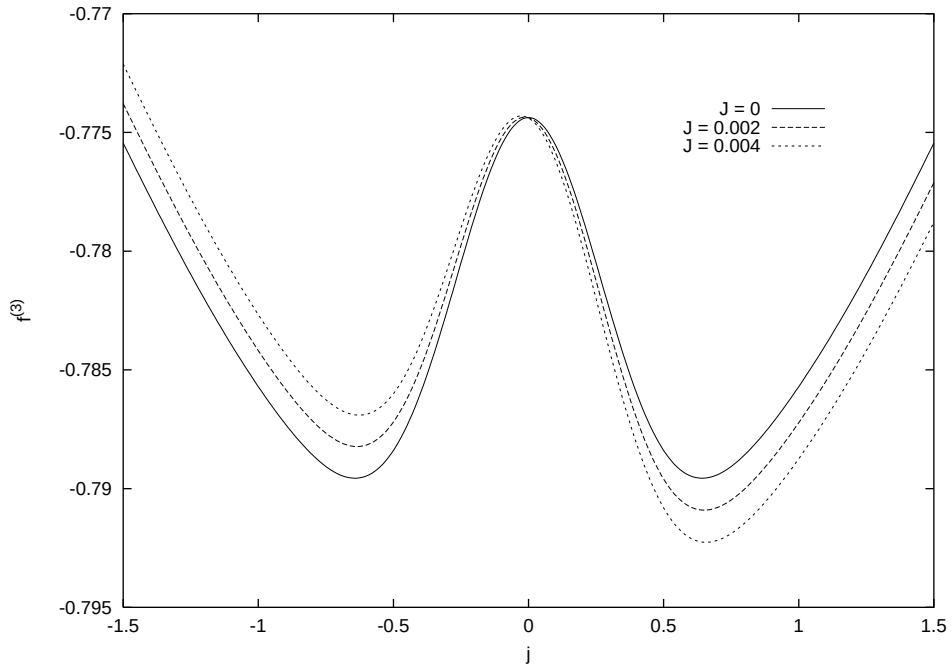

Figure 2: Plots of $f^{(3)}(J;j)$ vs. j for a 3D Ising model, at 3rd order. The inverse temperature is $\kappa = \kappa_c + 0.03$, i.e. the system is in the broken symmetry phase. The three curves correspond to three different values of J. Each curve consists of 300 calculated points, which are connected by straight lines. The lines appear smooth due to the fine resolution of the data points.

$J = 0.004$. With one local and one global minima, both in deep wells, we had to be careful to select the global minimum numerically.

3.1.3 Critical Point

The critical point, κ_c, was identified by searching for a small interval where $\bar{j}(\kappa_-) = 0$ and $\bar{j}(\kappa_+) \neq 0$ so that $\kappa_c = \frac{1}{2}(\kappa_+ + \kappa_-) \pm \frac{1}{2}(\kappa_+ - \kappa_-)$. In practice because the free energy is insensitive to changes in the variational parameter j (it is a minimum in j space) the minimum in variational parameter space is located to a much lower accuracy (in terms of the values for the variational parameters) as compared to the numerical accuracy of the routines. We need to know the variational parameters in order to find the critical point so uncertainties in these limit our knowledge of the critical point. This is discussed in detail in appendix D.

In table 1 we show the results obtained by searching for the critical inverse temperature at all orders of the 2D, 3D and 4D Ising models. Comparing these numerical values for the critical κ to those found exactly (see below in table 5), we find the numerics were accurate to a fractional error of $O(10^{-16})$, i.e. to the accuracy quoted. This provides a further check of our numerics. A more detailed discussion of the errors in numerical identification of the critical point is given in appendix D.

In figure 3 we plot the values of κ_c for all the orders. We also indicate the result $\kappa_c = 0.221654$ obtained by Monte Carlo methods for the same model [72, 73, 49]. The figure shows that if *only* the odd orders are considered, an imaginary line going through

Order	κ_c for 2D	κ_c for 3D	κ_c for 4D
1	0.2500000000000000	0.16666666666666667	0.1250000000000000
2	0.3333333333333333	0.20000000000000000	0.1428571428571429
3	0.3461538461538462	0.20270270270270270	0.1438356164383562
4	0.3768115942028986	0.20963172804532578	0.1464393179538616
5	0.3824833702882483	0.21006903118305165	0.1465228381635412
6	0.3944031482291211	0.21343833354502731	0.1475861410791982
7	0.3954564542557659	0.21353497619553782	0.1475854241672118

Table 1: Numerical results for the critical points in the 2D, 3D and 4D Ising models, at all orders up to 7. Accuracy is at least to the last digit quoted (16th).

the points seems to converge to a value close to the one predicted by Monte Carlo. The

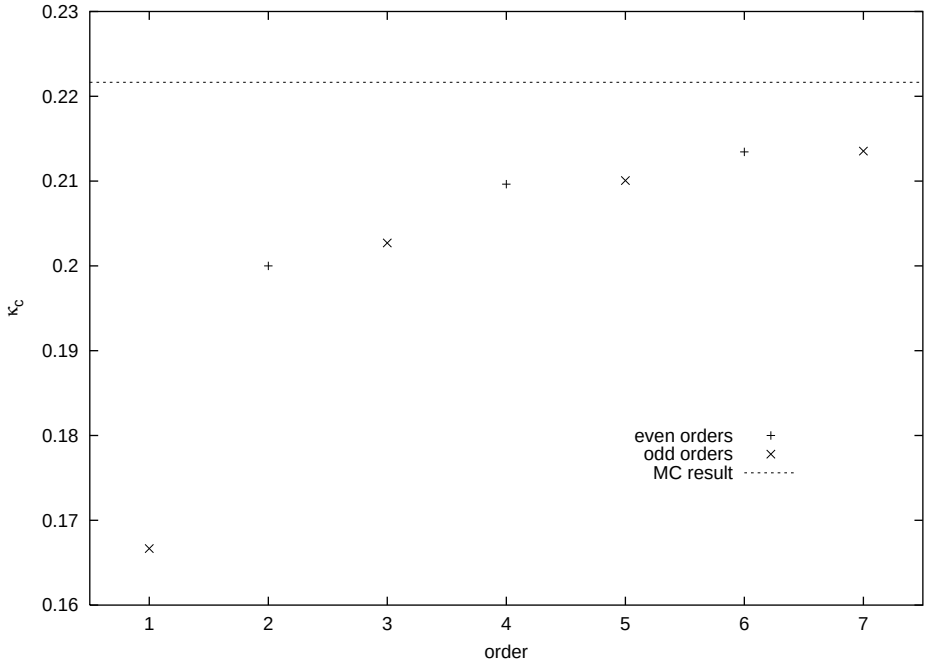

Figure 3: The plot shows the values of κ_c for the 3D Ising model, for all orders up to and including the 7th order. The Monte Carlo result is $\kappa_c = 0.221654$ [72, 73, 49].

even points also show a smooth progression and appear to be giving reasonable behaviour. However, in slightly more complicated models the even orders do not give critical points at all. Experience tells us to distrust the even orders of our model and we will concentrate on the odd orders only.

3.1.4 Field Expectation Value

Consider first the evaluation of the expectation value via direct numerical differentiation of the optimised free energy, $\left\langle \bar{\phi} \right\rangle^{(R)}_{\text{diff}}$ of (43). We present the results for orders 3, 5 and 7 in figure 4. We see that the expectation value displays similar behaviour for the three odd orders considered and qualitatively, the results are good. The expectation value clearly indicates the unbroken symmetry phase with a vanishing value. For $\kappa > \kappa_c$, we see the effect of spontaneous magnetisation. The only appreciable difference between the three

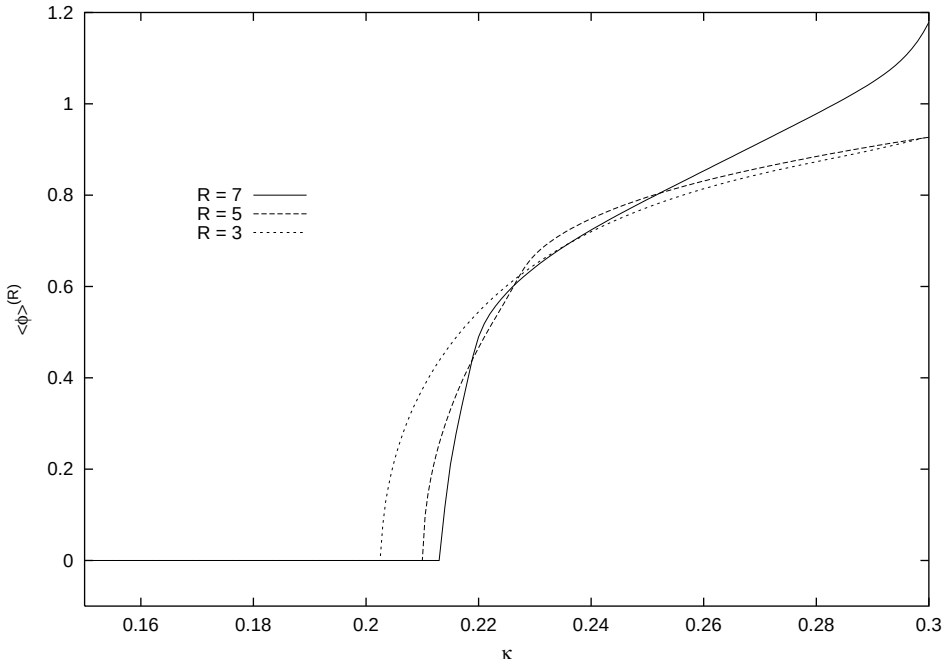

Figure 4: The plot shows $\left\langle \bar{\phi} \right\rangle^{(R)}_{\text{diff}}(\kappa, J = 0)$ vs. κ for $R = 3, 5, 7$, in the 3D Ising model. The physical source $J = 0$. The expectation value is calculated by direct numerical differentiation as given by equation (43). Each curve consists of 400 calculated points, which are connected by straight lines. The lines appear smooth due to the fine resolution of the data points.

orders is the position of the critical point. Overall, the plot demonstrates that the LDE can be used to model spontaneous symmetry breaking with the expectation value as an order parameter. We shall look later at the near-critical behaviour, when we analyse the critical exponents.

In figure 5 we have shown a plot of the expectation value calculated by optimising the free energy with respect to j first for a given κ and $J = 0$, but then substituting the optimal variational parameter $\bar{j}$ into the explicit expansion of $\left\langle \phi \right\rangle^{(3)}_{\text{expl}}(\kappa, J = 0; j)$ to produce $\left\langle \bar{\phi} \right\rangle^{(3)}_{\text{expl}}(\kappa, J = 0)$ (see equation (44)). In figure 5 we show a plot of $\left\langle \bar{\phi} \right\rangle^{(3)}_{\text{expl}}$ and $\bar{j}$ for a range of κ. These are results from a 3D, 3rd order run of the Ising model, again with the physical source $J = 0$. In broad terms, from the curve of $\left\langle \bar{\phi} \right\rangle^{(3)}_{\text{expl}}$ we clearly see again a phase transition at a point which we denote by κ_c, the critical inverse temperature. The critical points are the same for both approaches.

By clearly acquiring a zero and non-zero value, depending on the phase, the expectation value is an order parameter of the model. Additionally, we find that the same is true for the variational parameter j. Thus we can use either order parameter to find the value of κ_c by searching for the inverse temperature at which $\left\langle \bar{\phi} \right\rangle^{(R)}$ or $\bar{j}$ switch from a zero to a non-zero value.

Note that the 3rd order curves using both methods look the same for both methods. In fact, accurate numerical comparison of the two methods reveal differences of $\sim 10^{-20}$. Since we used $\epsilon = 10^{-20}$ to calculate the numerical derivative (see equation (43)), this discrepancy is of purely numerical nature.[10] It is remarkable that the two methods

[10]The same numerical calculation was done for the 5th and 7th orders too.

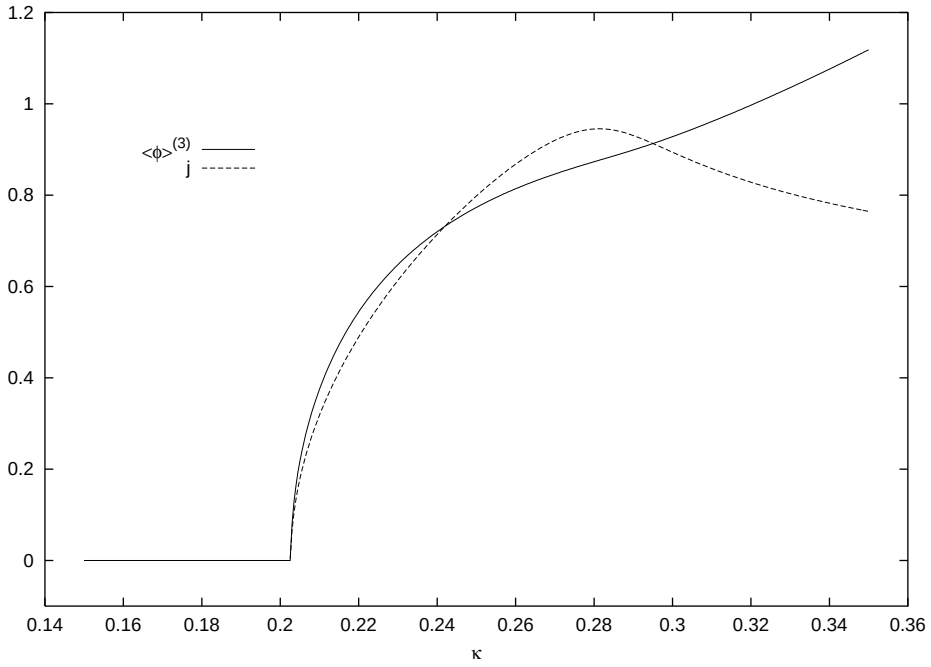

Figure 5: Plot of $\left\langle \bar{\phi} \right\rangle^{(3)}_{\text{expl}}$ and $\bar{j}$ vs. κ for the 3D Ising model at 3rd order, with the physical source $J = 0$. Each curve consists of 300 calculated points, which are connected by straight lines. The lines appear smooth due to the fine resolution of the data points.

produce the same results, especially considering how different the results will be for the susceptibility, discussed in the next section.

3.1.5 Susceptibility

As with the field expectation value, the susceptibility is another quantity that we can access by using optimised variational parameters or by direct numerical differentiation of the free energy density. The susceptibility is given by the second derivative:

$$\bar{\chi}^{(R)}_{\text{diff}} = -\frac{\partial^2 \bar{f}^{(R)}}{\partial J^2} \approx -\frac{\bar{f}^{(R)}(J+\epsilon) - 2\bar{f}^{(R)}(J) + \bar{f}^{(R)}(J-\epsilon)}{\epsilon^2} \tag{55}$$

where the right hand side defines the direct numerical differentiation approach. The other approach is based on a function $\chi^{(R)}_{\text{expl}}(\kappa, J; j)$, which will assume the 'correct' value once an optimised $\bar{j}$ is substituted, i.e. $\bar{\chi}^{(R)}(\kappa, J) = \chi^{(R)}(\kappa, J; \bar{j})$.

Figure 6 shows a plot of four different $\bar{\chi}^{(R)}(\kappa, J = 0)$ curves. Three of those are $\chi^{(R)}_{\text{expl}}(\kappa, J)$ calculated by optimising j first from the free energy, and then substituting this optimised value into $\chi^{(R)}$, for $R = 3$, $R = 5$ and $R = 7$. The fourth curve shows $\bar{\chi}^{(3)}_{\text{diff}}(\kappa, J = 0)$ as calculated through direct differentiation (55). This plot leads to important conclusions about the methods used to calculate each curve, and we shall discuss these in what follows.

The curve denoting the direct numerical differentiation approach $\bar{\chi}^{(3)}_{\text{diff}}$ encapsulates the correct qualitative behaviour of the susceptibility. It *is* the case that χ blows up at the critical point, due to correlations extending over the whole lattice (system). This is due to the fact that this approach is capturing the non-smooth nature of the field expectation value apparent in figure (4). The $\chi^{(R)}_{\text{expl}}(\kappa, J)$ form has only finite peaks at all

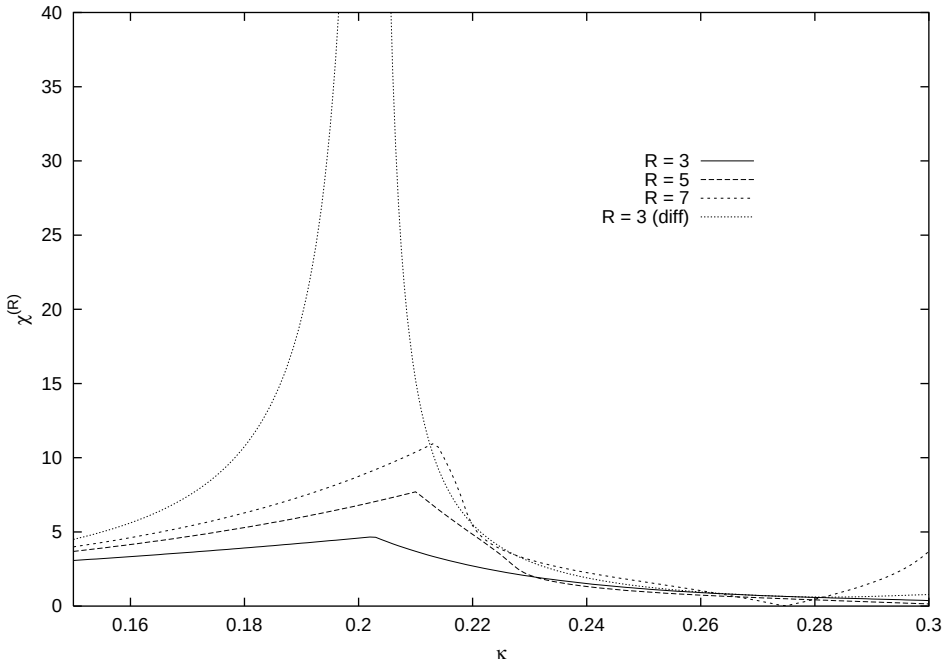

Figure 6: The plot shows $\bar{\chi}^{(R)}_{\rm expl}(\kappa, J=0)$ vs. κ for $R = 3, 5$ and 7 in a 3D Ising model. These three curves are calculated using a previously optimised j. The '$R = 3$ (diff)' curve is $\bar{\chi}^{(3)}_{\rm diff}(\kappa, J=0)$ calculated using direct differentiation, as given by equation (55). Each curve consists of 200 calculated points, which are connected by straight lines. The lines appear smooth due to the fine resolution of the data.

three orders, with the peaks getting larger as the order increases. The fact that the peaks shift towards higher κ is purely due to the value of κ_c shifting at each respective order (see table 1). It is easy to see (mathematically) why the peaks in the forms $\chi^{(R)}_{\rm expl}(\kappa, J)$ become more pronounced at higher orders. The explicit expressions for $\chi^{(R)}(\kappa, J; j)$ are a sum of a finite number of terms, each a product of I_p factors, physical and variational parameters. Like the expressions obtained in a high temperature expansion on the lattice, these expressions can not become infinite. Physically, this is a reflection of the fact that at, for example, 3rd order, our method can only correlate lattice sites spaced no more than three sites apart. Diagrammatically, at 3rd order, two sites i and j, sitting three sites apart from each other can be correlated only through the diagram:

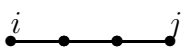

(56)

If i and j happen to be further apart, the method will never be able to correlate them. The situation for $R = 5$ and $R = 7$ is analogous: the method can only correlate lattice sites which are within R sites of each other and they can never see the infinite correlation length near the critical point. This is the reason why the $\chi^{(R)}_{\rm expl}$ peaks grow as orders increase, but still remain finite for finite R.

3.1.6 Critical Exponents

The β critical exponent is defined in terms of the *reduced inverse temperature* κ_r

$$\lim_{\kappa \to \kappa_c} \left(\langle \bar{\phi} \rangle \right) \propto \left| \frac{\kappa - \kappa_c}{\kappa} \right|^{\beta} = |\kappa_r|^{\beta}, \quad \kappa_r := \frac{\kappa - \kappa_c}{\kappa} \tag{57}$$

Let us take the three-dimensional order seven results as a prototypical example. Using data produced with 155 digit accuracy, we fit

$$\left\langle \phi \right\rangle^{(fit)} = A \left|\kappa_r\right|^{\beta} \left|\ln(\kappa_r)\right|^{c} \tag{58}$$

using 30 digit accuracy on the fitting for 100 values of $\kappa \in \langle \kappa_c, \kappa_c + 10^{-10}]$. The best fit is for $\beta = 0.5 + 3 \times 10^{-10}$ and $(\kappa_c/\kappa_{c,\text{exact}} - 1) = 1.4 \times 10^{-20}$ with $\chi^2 = 8 \times 10^{-20}$ as figure 7 shows. The reference value $\kappa_{c,\text{exact}}$ is given later in table 5. The fit is very good so

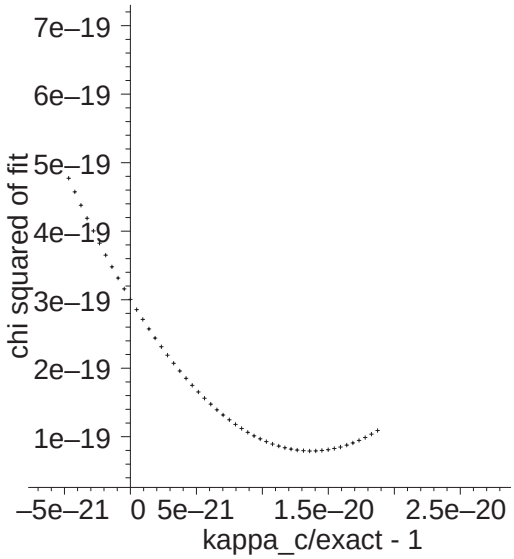

Figure 7: Plot of the standard statistical measure χ^2 for the best fit of (58) to the behaviour of the 3D Ising model 7th order results near critical point for a fixed $(\kappa_c/\kappa_{c,\text{exact}} - 1)$.

the fact that β is not exactly a half looks significant at first given the high calculational accuracy.

However the fractional differences between this best fit curve and the data points are shown in figure 8. This shows a small but significant systematic error that we have not been able to eliminate, perhaps due to a poor choice for the form of the fitting function (58). There is no reason why our approximate form should have exactly the same functional form as the full solution and we are working here to high levels of numerical accuracy. Fitting data in the same way but in the ranges $\kappa \in \langle \kappa_c, \kappa_c + 10^{-r}]$ for $r = 6$ and 8 reveals that the all the errors and the deviation of the best estimate for $(\beta - \frac{1}{2})$ reduce by two orders of magnitude as we use data ranges with $r = 6, 8$ and then 10, closer and closer to the critical point. If we fit a pure power law ($c = 0$ in (58)) then the fit is slightly worse, the beta is different and again differs by the same order of magnitude from 1/2. Attempts to fit forms for other corrections to (57) to the data produce similar results but no consistency in any shift of β from one half. Thus, despite our high numerical accuracy, we conclude that the deviation from $\beta = \frac{1}{2}$ is not significant and that our data is consistent with $\beta = 1/2$, again to about nine significant digits.

Power law behaviour of the susceptibility near the critical point defines the γ critical exponent as

$$\chi \propto \left|\kappa_r\right|^{-\gamma} \tag{59}$$

To find the value of γ, we used the susceptibility $\chi^{(R)}_{\text{diff}}$ calculated by direct differentiation of the free energy density (55). Following our experience with β we merely fitted the

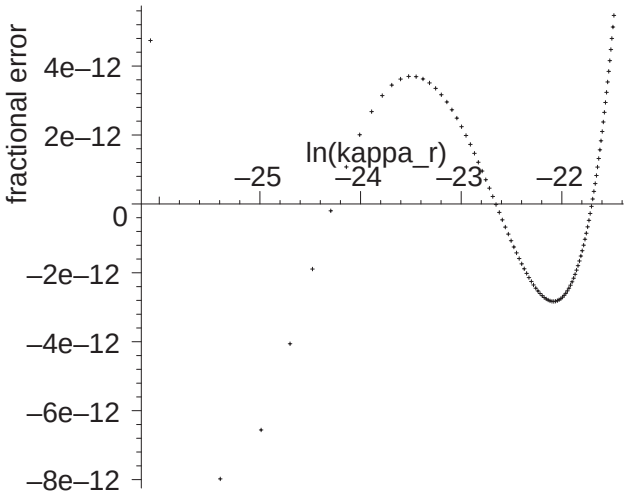

Figure 8: For the best fit of the critical behaviour of the 3D Ising model 7th order results ($J = 0$), a plot of $\ln(\langle\bar{\phi}\rangle^{(\mathrm{fit})})/(\langle\bar{\phi}\rangle^{(7)})$ vs. $\ln|\kappa_r|$ for $\kappa \in (\kappa_c, \kappa_c + 10^{-10}]$ with $\beta = 0.5 + 3 \times 10^{-10}$ and $(\kappa_c/\kappa_{c,\mathrm{exact}} - 1) = 1.4 \times 10^{-20}$.

simple power law form (59) to the data for $\ln\left|\bar{\chi}^{(3)}\right|$ with κ taken in the broken phase and $\kappa \in (\kappa_c, \kappa_c + 10^{-8}]$. The result is $\gamma = 1 * (1 \pm 10^{-8})$ for orders 3, 5 and 7.

Finally the δ critical exponent is defined by the following power law

$$\langle\phi\rangle \sim |J|^{\frac{1}{\delta}} \qquad \text{for } \kappa_{\mathrm{r}} = 0 \tag{60}$$

Note that the δ critical exponent has nothing to do with the bookkeeping parameter δ defined in the LDE methodology. Again we fitted the power law form (60) to the data for $\langle\phi\rangle_{\mathrm{diff}}$ with $\kappa = \kappa_c$. The result of the fit at orders 3, 5 and 7 is $\delta = 3 * (1 \pm 10^{-8})$, to similarly high accuracies as for the other critical exponents.

A summary of the critical exponents for the Ising model, as found by our LDE method is shown in table 2. For comparison, we give the values of the same critical exponents

Exponent	LDE	MC+HT
β	0.5	0.3485
γ	1	1.3177
δ	3	4.780
$\delta/(\gamma/\beta + 1)$	1	1.000

Table 2: The values of the three critical exponents β, γ and δ for the Ising model in three dimensions. First as obtained by our LDE study (at orders 3, 5 or 7) secondly by a combination of Monte Carlo and high-temperature expansions [57, 58].

as found by [58], using a combination of Monte Carlo simulations based on finite-size scaling methods, and high-temperature expansions. We note that the values obtained by the LDE match those predicted by mean field theory up to errors.

One final test is to check the universal relationship $\delta = 1 + (\gamma/\beta)$ but as mean field values satisfy this, our values also satisfy this requirement within the accuracy of our measurements.

3.1.7 The Ising model in other dimensions

So far we have given a detailed description of our results for the 3D Ising model. In table 5 we list critical inverse temperatures for all orders of the 2D, 3D and 4D Ising models. Again these are exactly solvable so can be used to check our numerical calculations. The critical exponents can then be measured as already described. Again they are identical to the 3D results, that is mean field values at orders 3, 5, 7 within the accuracy of our calculations. This independence of critical exponents with dimension is also characteristic of mean field theory but is not seen in the true results.

3.1.8 The Ising model and other optimisation schemes

Once the complete expressions have been obtained for the various scalar field models, it is relatively quick to compute them for a range of values in the Ising model with its single variational parameter and with I_p 'integrals' being given by simple functions. It is an ideal place to illustrate other aspects of the LDE method. We will just study the $J = 0$ case.

First let us look at optimisation scheme known as FAC - fastest apparent convergence. In this scheme one chooses the variational parameters such that the last term in the delta expansion (or sometimes the last r terms) is zero. The idea is that in well behaved series the last term can often be used to get an idea of the error due to truncation of the series so the 'optimal' result is where this is zero.

The modulus of the fractional contribution to the free energy from each order in the full delta expansion is plotted in figure (9) for the seventh order calculation. The spikes

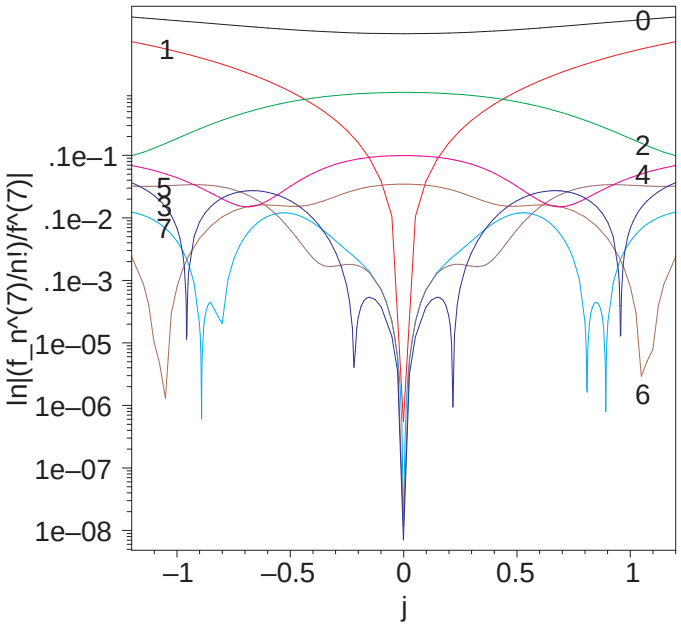

Figure 9: The eight terms in the delta expansion of the free energy of the Ising model in three dimensions up to order seven with $J = 0$ and $\kappa = 0.23061777$. Normalised with respect to the total free energy, the log of the absolute value is plotted. The numbers on one end of every curve indicate the order of the term plotted. Note that most spikes represent points where a term is going to zero but numerical and plotting limitations mean the curves are of finite extent. Likewise, the curves ought to be exactly symmetric about $j = 0$ but near the spikes numerical limitations prevent this appearing on the plot.

ought to be going to minus infinity on this log plot as these are points where a term goes through zero.

It is clear that the odd terms always go to zero at $j = 0$. This should be expected as all the odd integrals I_p are zero when $j = 0$, and at odd orders, for a trial action S_0 made up of only odd powers of fields, every contribution in the sum of such contributions making up the odd order expression must contain at least one I_p with p odd. Thus only an FAC procedure based on odd terms alone, will provide a suitable unbroken $j = 0$ solution. Thus let us further confine ourselves to an FAC procedure where we demand that the optimal variational parameters $\bar{\boldsymbol{v}}$ are such that the last term in the expansion is zero

$$f^{(R)}_{\rm FAC}(\boldsymbol{p}) := \sum_{n=0}^{R} \frac{\delta^n}{n!} f_n(\boldsymbol{p}, \bar{\boldsymbol{v}}), \quad f_R(\boldsymbol{p}, \bar{\boldsymbol{v}}) = 0 \tag{61}$$

Now we notice that, at least for the value of κ used in figure (9), there are in fact non-zero values of j which satisfy the FAC optimisation criterion (61). There are four: two positive j and the same solutions with opposite sign (as there must be under the Z_2 symmetry at $J = 0$). Further investigation shows that these two new solutions appear first at $\kappa^{(7)}_{{\rm FAC},C} = \kappa^{(7)}_C * (1.048 \pm 0.002)$ where $\kappa^{(7)}_C \approx 0.2135$ is the critical κ value found in the same model but using the minimum free energy criterion (7). Now the problem for $\kappa > \kappa^{(7)}_{{\rm FAC},C}$ is which minimum to choose — we have three distinct possibilities after symmetry is taken into account. This illustrates a general problem when using criteria such as FAC and PMS. They often present multiple possible solutions for the optimal variational parameters and one must use further criteria, sometimes no more than physical intuition, to choose one solution. The minimum free energy method we use guarantees a unique answer, up to symmetry, except at transition points.

To finish with FAC, let us choose the j solution that has the lowest free energy as well as satisfying (61) for this seventh order $J = 0$ example. As figure (9) shows this is the smallest non-zero j solution (the free energies are negative, so this has the largest free energy ratio when compared to the $j = 0$ solution). This solution appears at about

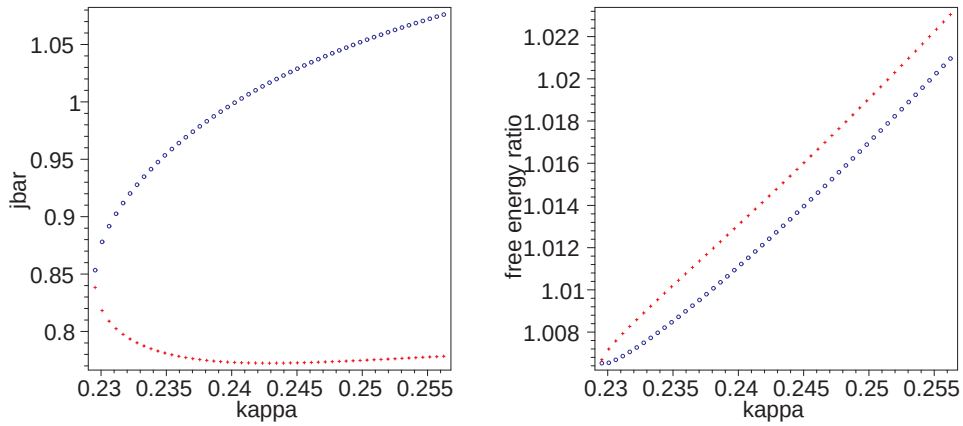

Figure 10: The optimal non-zero j solutions (left hand plot) and the resulting free energy normalised to the free energy at $j = 0$ (right hand plot) for the Ising model in three dimensions at order seven with $J = 0$. Note the smaller j solution (crosses) has the most negative free energy.

$\bar{\jmath} \approx 0.85$ at $\kappa = \kappa^{(7)}_{{\rm FAC},C}$ and so this FAC criterion is giving us a *first order transition*. Any physical quantity we calculate will suddenly change in value as we increase κ through

$\kappa^{(7)}_{\mathrm{FAC},C}$ as the j parameter is suddenly changed from 0 to around 0.85. In some models this is a good thing. For instance in the Electroweak model for some parameter ranges we expect a first order transition and this sudden change in the optimal variational parameter solution can give this behaviour in LDE as obtained in [47, 48]. However, we are expecting a second order transition in this model. Our conclusion is that FAC is an unsatisfactory optimisation scheme for the optimised hopping parameter expansion of the Ising model.

We next turn to PMS. In this scheme, one looks for turning points *in the quantity of interest*. Thus for a fixed set of physical parameters $\boldsymbol{p}$ the optimal values chosen for the variational parameters $\boldsymbol{v}$ will vary as we study different quantities. This is a standard procedure when PMS is applied to issues such as scheme dependence in particle physics [74, 9].

First let us apply PMS to the free energy. The plot in figure 1 shows how this works. For $\kappa < \kappa_c$ there is a single turning point at $j = 0$ at the global minimum of the free energy so the PMS gives the same answer as free energy minimisation in the unbroken phase. However for $\kappa > \kappa_c$ there are three turning points and in principle PMS does not distinguish between turning points in the variational parameter space. In practice one often chooses the flattest turning point (for least sensitivity to unphysical parameters) but here there is little to choose between them. Failing this, with PMS one often falls back on choosing the turning point which makes the most physical sense. Here that might be the ones with the lowest free energy or with $j \neq 0$ since we are expecting symmetry breaking. Of course with such additional arguments one selects the same solution as we had when simply searching for the minimum of the free energy. In this sense PMS is working here as well as the minimum free energy criterion. What it does highlight is that PMS need not give a unique solution nor a single solution.

More interestingly we can try the PMS on other quantities. Let us look at the expectation value of ϕ as a function of variational $\boldsymbol{v} = \{j\}$ and physical parameters $\boldsymbol{p} = \{\kappa, J = 0\}$. This is shown in figure 11. The main point to note is that $\langle\phi\rangle$ is an odd

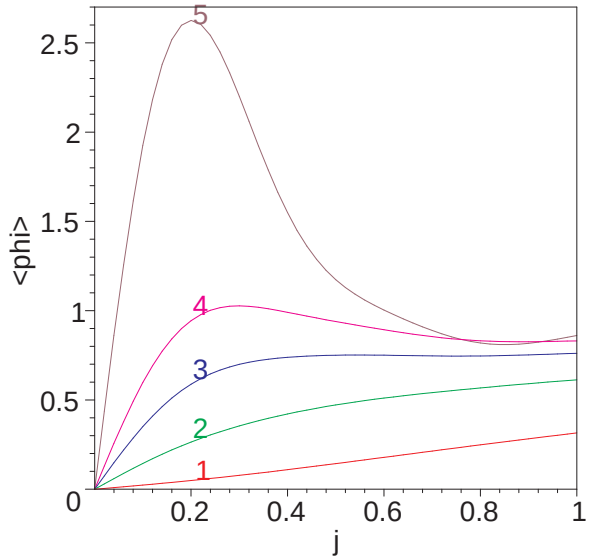

Figure 11: $\langle\phi\rangle(\kappa, j)$ in the three dimensional Ising model at order seven with $J = 0$ and fixed κ. The labels indicate that $(\kappa - \kappa_c) = -0.05$ (1), 0.0 (2), +0.03 (3), +0.05 (4) and +0.1 (5). Note that the new turning points appear at a kappa about 14% higher that κ_c, the value shown with curve three. The curves are all odd in j so negative j are not displayed.

function of j and for large ranges of κ, the low kappa regions, there are no turning points in ϕ. For larger ϕ's there are four turning points, with one nice shallow local minimum as a function of j (maximum for negative j) appearing at some $\kappa \neq \kappa_c$. However it is clear that the PMS fails to give reasonable qualitative behaviour for this quantity.

Thus for the Ising model, the FAC fails to work at all, while the PMS fails when applied to some quantities, and works on others[11] if implemented with some extra reasonable but ad-hoc criteria. On the other hand the unambiguous minimum free energy principle gives great qualitative behaviour for all quantities (when calculated using derivative of the optimised free energy) but it produces poor critical behaviour of a type seen in the mean field approximation.

3.2 Spin-1 Model

The spin-1 model differs from the Ising model in that ϕ can acquire the values ± 1 and 0. This means that a quadratic ultra-local term is no longer redundant (as it was for the Ising model), so S and S_0 are (c.f. equation (8)):

$$S = -\kappa \sum_{i\in\Lambda} \sum_{j\in\mathcal{N}_i^+} \phi_i\phi_j + \sum_{i\in\Lambda} \left[J\phi_i + \alpha\phi_i^2\right] \tag{62}$$

$$S_0 = \sum_{i\in\Lambda} \left[j\phi_i + k\phi_i^2\right] \tag{63}$$

Thus the I_p integrals (15) are again simple functions

$$I_p(j,k) := \begin{cases} 1 + 2e^{-k}\cosh(j) & (p=0) \\ 2e^{-k}\cosh(j) & (p \text{ even and positive}) \\ -2e^{-k}\sinh(j) & (p \text{ odd}) \end{cases} \tag{64}$$

However, now we are optimising in the two-dimensional variational space of $\boldsymbol{v} = (j,k)$. We set the parameter $\alpha = \ln 2$ [49, 50].

The optimisation with respect to two parameters causes no additional problems at odd orders. The j parameter acts as an order parameter as before. At low values of κ $k = 1$ and $j = 0$ gives the lowest free energy, i.e. where the variational parameters equal the physical parameters $\boldsymbol{v} = \boldsymbol{p}$ and the trial action exactly equals the ultra-local part of the physical action. However, the gradient in the free energy with respect to j slowly decreases and becomes zero at some point and this is the critical point. For higher κ values there are a pair of minima at $j \neq 0$ and $k \neq 1$. The free energy as a function of the variational parameters is shown for the third order in figure (12) for values of kappa either side of this critical point.

Table 3 summarises the critical inverse temperatures found for the 2D, 3D and 4D cases. Exact expressions can be obtained but they involve integer powers of $1/e$ and are not given here.[12]

The critical exponents behave in the same way as for the Ising model: $\beta = 0.5$, $\gamma = 1$ and $\delta = 3$ to over eight significant digits, irrespective of order or dimension.

We present only odd orders, as the even orders do not produce good behaviour in the variational space. It is the behaviour in the quadratic variational coefficient, k which leads to the even orders failing to produce good minimum energy values. For instance

[11] Presumably PMS works for those quantities even in j.

[12] This is because in the unbroken phase, the coefficient of the quadratic term k prefers to be equal to that in the physical action, here chosen to be 1. Thus the I_p integrals contain $1/e$ factors.

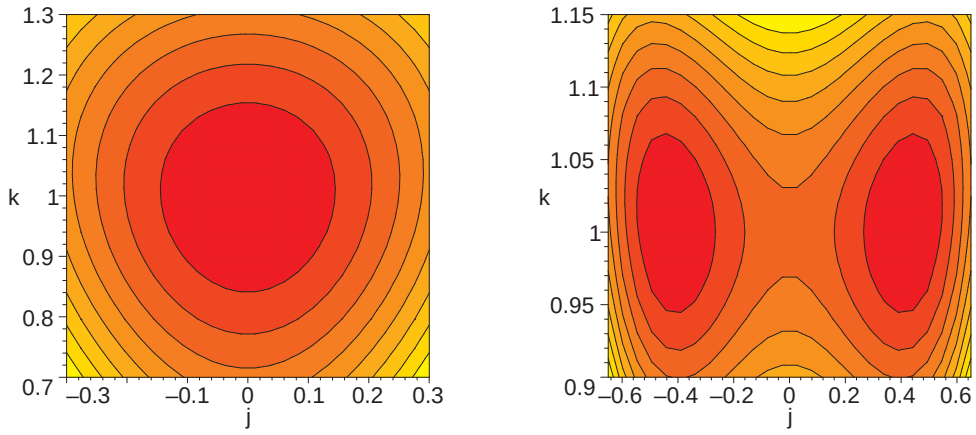

Figure 12: Contours of constant free energy (highest values at edges of plot) for the spin one model in three dimensions at order 3 for $\kappa = 0.9\kappa_c$ (left) and $\kappa = 1.1\kappa_c$ (right). Here κ_c is a genuine critical point.

Order	κ_c for 2D	κ_c for 3D	κ_c for 4D
1	0.5000000000000000	0.3333333333333333	0.2500000000000000
3	0.5753424657534247	0.36464088397790055	0.2670623145400593
5	0.6060227414719480	0.37172944976396613	0.2697296215999957
7	0.6475789767717944	0.37519182797115188	0.2700940775993100

Table 3: List of all critical points for the 2D, 3D and 4D spin-1 models, at all odd orders up to 7. The values are obtained by using the linear and quadratic variational parameters, j and k. The result obtained by Monte Carlo methods for the 3D case is $\kappa_c = 0.383245$ [49].

in figure (13) the free energy of the spin one model at second order is shown. The free energy behaves reasonably as a function of κ and we can identify a value κ_c where where the second derivative with respect to j is zero at $j = 0, k = 1$. However, there, as for all values shown the free energy has no turning point with respect to k and no obvious minimum.

Interestingly, we tried reducing the number of variational parameters to one, namely, we used j only. The results produced in this way were the same as with the k variational parameter included, for all cases. The only differences occurred at even orders, at which we could not find any reliable results anyway.

3.3 ϕ^4 Model

As a reminder, the action and the trial action of the ϕ^4 model are given by

$$S = -\sum_{i\in\Lambda}\sum_{j\in\mathcal{N}_i^+}\phi_i\phi_j + \sum_{i\in\Lambda}\left[J\phi_i + \alpha\phi_i^2 + g\phi_i^4\right] \tag{65}$$

$$L_0(\phi_i, \boldsymbol{v}) := \left[j\phi_i + k\phi_i^2 + l\phi_i^4\right] \tag{66}$$

Thus the I_p integrals (15) are now non-trivial and we are optimising in the two-dimensional variational space of $\boldsymbol{v} = (j, k)$ if we set $l = g$ or more generally we work with a three dimensional variational space $\boldsymbol{v} = (j, k, l)$. Note that here the inverse temperature κ has

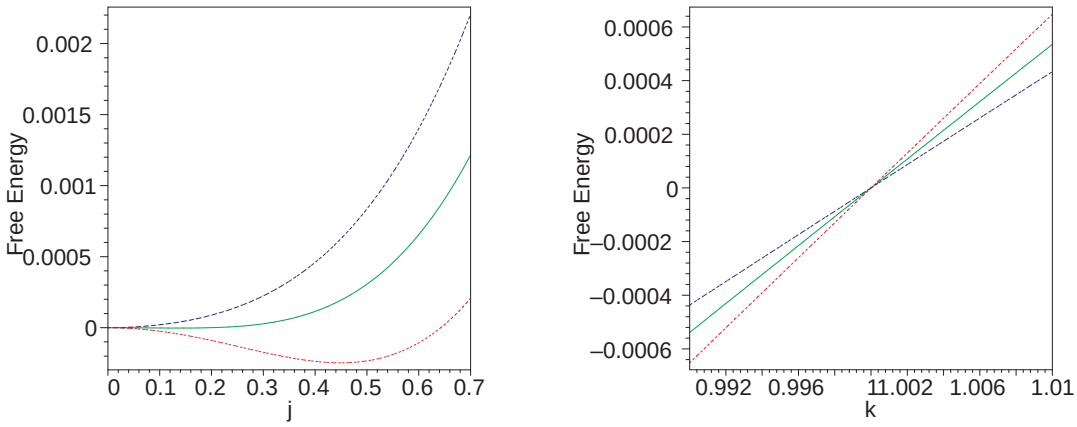

Figure 13: The free energy of the spin one model in three dimensions at order 2 at $\kappa/\kappa_c = 0.9$(top blue curve), 1.0 (middle green continuous curve), 1.1 (bottom red dashed curve). At order 2, κ_c is the point where the second derivative of the free energy with respect to j is equal to zero at $j = 0, k = 1$, as the left hand graph indicates (its for $k = 1$). The figure on the right is at $j = 0$ and shows that it is the lack of a turning point in the k variational parameter which prevents the method working at order 2. (Tim Maple analysis)

been scaled to unity when discretizing the ϕ^4 action (c.f. section 2.2). Instead, we use α, the lattice *mass parameter*, as the physical basis for 'driving' the system through the phase transition, so we have physical parameters $\boldsymbol{p} = (J, \alpha, g)$. We set $g = 25$, to agree with [45, 18].

The crucial difference in this model as compared to the Ising and spin-1 models, is the number of degrees of freedom of the field. For the ϕ^4 model, the field is a continuous parameter, and the trace in the partition function becomes an integral. Therefore, the numerical calculation of the I_p factors is a computationally intensive task as they are now integrals whereas they were standard functions for the previous two models. We had to make sure that the accuracy of our numerical integration was appropriate given the accuracy problems encountered in manipulating the long expressions the LDE gives for the quantities of interest. For instance, when 256-bit arithmetic was used (which gives approximately 77 decimal places of accuracy), we ensured that the integrals were always evaluated to a precision of at least 70 decimal places.

Table 4 summarises the critical values of α at odd orders for the 2D, 3D and 4D cases. The critical values were calculated using only the linear and quadratic variational param-

Order	α_c for 2D	α_c for 3D	α_c for 4D
1	-14.585428484653014	-10.007548118296870	-6.956574606584720
3	-18.407621223877752	-11.560051936952422	-7.887721708383015
5	-20.106877371919612	-11.918151992492446	-8.018314178185453
7	-21.240866931195218	-12.138250831659820	-8.062177866626536

Table 4: List of critical α_c for the 2D, 3D and 4D ϕ^4 model, at all odd orders up to 7. The values are obtained by using the linear and quadratic variational parameters, j and k.

eters. The critical exponents β, γ and δ turned out to be 0.5, 1 and 3, respectively, again

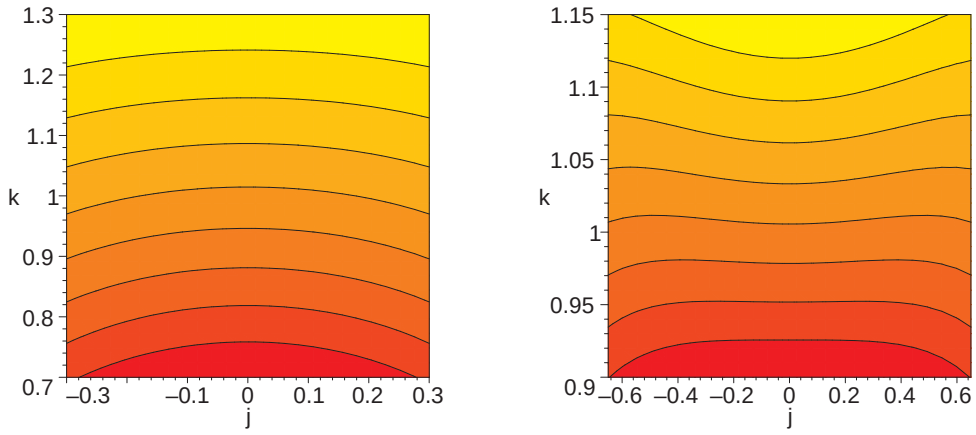

Figure 14: The free energy of the spin one model in three dimensions at order 2 at $\kappa = 0.9\kappa_c$ and $\kappa = 1.1\kappa_c$. Here κ_c is the point where the second derivative of the free energy with respect to j is zero at $j = 0, k = 1$. It shows that it is the behaviour with respect to the k variational parameter which stops the method working at order 2. (Tim Maple analysis)

reproducing the values found in the Ising and spin-1 models to at least eight significant figures.

The 3rd order result in 4D successfully reproduces and refines the result $\alpha_c = -7.88$ found by a similar variational cumulant approach in [18]. Two other studies of the 4D theory, based on Monte Carlo methods [75, 76] found $\alpha_c = -8.2$ and $\alpha_c = -8.275$, respectively. A crude extrapolation of the trend of our 4D results, as given in table 4, gives a critical value of $\alpha_c \approx -8.08$.

Remarkably, even in this model, the results using the linear variational parameter only are no different. The critical mass parameters α_c, at all orders and in all dimensions are the same. We also found that including the quartic parameter made no difference to the critical behaviour.

4 Exact Analysis of Ising Model case

In this context, exact means no numerical evaluations were used. The approximate algebraic forms produced for the free energy were solved algebraically, including the optimisation aspect. This is possible only for Ising model where there is a single variational parameter j.

4.1 First order

The lowest order, $R = 1$, LDE approximation to the Ising model is easily calculated. The derivation also provides a simple concrete example of the LDE method. For the free energy we find that

$$f^{(1)} = -\ln \mathcal{Z}_0 - \langle \Delta S \rangle_{\mathrm{C}} \tag{67}$$

$$= -\ln \mathcal{Z}_0 - \kappa d \langle \phi \rangle_0^2 - (j - J)\langle \phi \rangle_0 \tag{68}$$

We are using statistical averages with respect to the S_0 action, defined in (13) so that

$$Z_0 = I_0, \quad \langle \phi^p \rangle_0 = \frac{I_p}{I_0} \tag{69}$$

They also factorise in the same way as the $\langle Q \rangle_1$ expectation values (29). Note the absence of quadratic and quartic terms from $\langle \Delta S \rangle_{\rm C}$ because of the simple form of the action and trial action for the Ising model. To find the minimum, we need to differentiate with respect to the sole variational parameter j, and set the resulting equation to zero. Using (48) we find that

$$\frac{\partial f^{(1)}}{\partial j} = \left(2\kappa d \langle \phi \rangle_0 + j - J\right) \left(\langle \phi^2 \rangle_0 - \langle \phi \rangle_0^2\right) \tag{70}$$

We set the above equation to equal zero, and provided $\langle \phi^2 \rangle_0 \neq \langle \phi \rangle_0^2$, the optimum j value, $\bar{\jmath}$, is found by solving

$$\bar{\jmath} = J - 2\kappa d \langle \phi \rangle_0 \tag{71}$$

The equation is generally transcendental since $\langle \phi \rangle_0$ depends on j.

For the Ising model, using the form of the I_p given in (54), it is possible to write this equation as

$$\bar{\jmath} = J + 2\kappa d \tanh(\bar{\jmath}) \tag{72}$$

In general this equation has three real solutions. If we wish to use the principle of minimum free energy we have to pick a solution which actually produces a minimum.

However, one can quickly see that for $J = 0$ then there is only one solution in the region $\kappa \leq \kappa_c = 1/(2d)$ and that is $j = 0$. Further, $\partial^2 f^{(1)}/\partial j^2 = 0$ at $\kappa = \kappa_c$ where the $j = 0$ solution turns from a global minimum into a local maximum (as happens at higher odd orders, see figure 1), and the correct value of $\bar{\jmath}$ is a non-zero one for $\kappa > \kappa_c$.

One can now see what the critical exponents are. First let us note that the delta expansion for $\langle \phi \rangle$ in the Ising model gives to lowest order

$$\begin{aligned} \langle \phi \rangle &= \langle \phi \rangle_0 + (j - J)\left(\langle \phi^2 \rangle_0 - (\langle \phi \rangle_0)^2\right) + d\kappa \left(\langle \phi^2 \rangle_0 \langle \phi \rangle_0 - (\langle \phi \rangle_0)^3\right) && (73) \\ &= -\tanh(j) + ((j - J) + d\kappa \tanh(j))\left(1 - \tanh^2(j)\right) && (74) \end{aligned}$$

Near the critical point we expect $\bar{\jmath}(J)$ to be small as $J \to 0$, $\kappa \to \kappa_c = 1/(2d)$. Normally we consider the optimal variational parameter j to be a function of the two physical variables κ and J. To solve analytically, however, its easiest if we express the relationship the other way round, i.e. making expansions in terms of $\bar{\jmath}$ and express the one physical parameter we vary in any critical exponent expression in terms of $\bar{\jmath}$. Thus keeping $\kappa = \kappa_c$ and studying $J(\bar{\jmath})$, $f(J(\bar{\jmath}))$, $\langle \phi \rangle(\bar{\jmath})$ in terms of a small $\bar{\jmath}$ expansion, we find that $J = \bar{\jmath}^3/3 + \ldots$ and $\langle \phi \rangle = -\bar{\jmath}/2 + \ldots$ showing that the critical exponent δ of (60) is 3. Likewise, for $J = 0$ we find that $(\kappa/\kappa_c - 1) = \bar{\jmath}^2/3 + \ldots$, $\langle \phi \rangle = -\bar{\jmath}/2 + \ldots$ and so the exponent β of (57) is 1/2.

The exact same exponents are obtained in an analytical mean field analysis. So is the LDE using minimum free energy optimisation the same as Mean Field theory? The answer is not exactly. In mean field theory for the Ising model on a simple hypercubic lattice we would write

$$\begin{aligned} Z &= \int D\phi \exp\{\kappa \sum_{i \in \Lambda} \sum_{j \in \mathcal{N}_i^+} \phi_i \phi_j - J \sum_{i \in \Lambda} \phi_i\} && (75) \\ \approx Z_{\rm MF} &:= \int D\eta \exp\{\kappa N d v^2 - JNv + 2dv\kappa \sum_{i \in \Lambda} \eta_i - J \sum_{i \in \Lambda} \eta_i\} && (76) \\ &= 2Z_0 \cosh(2d\kappa v - J) && (77) \end{aligned}$$

where $\eta_i = \phi_i - v$ and v is defined, self-consistently, to be the expectation value of the field, i.e.

$$v = \frac{1}{Z_{\rm MF}} \frac{\partial Z_{\rm MF}}{\partial J} = \tanh(2d\kappa v - J) \tag{78}$$

Comparing the variational parameter here, v with j of the our LDE calculation using lowest free energy optimisation, (72), we see that the two are related by

$$\bar{j} = J - 2d\kappa v \tag{79}$$

However, the forms for the expectation values $\langle\phi\rangle$ in the two calculations are clearly different as comparing (74) and (78), using (79) clearly shows. The difference though becomes negligible near the critical point which explains why the two approaches give the same answer for critical behaviour.

There is another way to view the link to mean field and that is to realise that mean field is merely another optimisation scheme within the LDE family. If we chose our S_0 to be

$$S_0 = \sum_{i\in\Lambda} L_0(\phi_i, \boldsymbol{v}), \quad L_0(\phi, \boldsymbol{v}) = \Omega + j\phi \tag{80}$$

rather than that of (12) we see that the LDE parameter j is playing the role of a mean field, and comparing (80) with (77), we obtain the relationship (79) but for all j values, not just the optimal values. If we used an optimisation scheme where

$$\bar{j} := 2d\kappa\langle\phi\rangle - J \tag{81}$$

then we would obtain MF as the zero-th order in this LDE scheme.

4.2 Exact results for κ_c

The Ising model can be solved exactly within the LDE approximation with minimum free energy optimisation at least at the orders and for the dimensions studied here. This was done using the algebraic forms for the diagrams produced by our nauty and MAPLE routines. Then by using the algebraic manipulation capabilities of MAPLE, we searched for the point where $\partial^2 f^{(R)}/\partial j^2 = 0$ at $j = 0$ as numerically we know this is where the critical point is. The exact values are given in table 5 as rationals, together with an eight digit approximate decimal value. The simple values obtained reflect the simple nature of the model. By way of comparison, in the spin-one model these fractions of integers are replaced by ratios of polynomials in $\exp\{-\alpha\}$ where α is the extra physical parameter of the spin-one model. The values of these integers for the Ising model results depend on the details of the lattice used. We have no explanation for the fact that the same numbers appear twice in the first column, once in the numerator, once in the denominator, though related behaviour is known for the LDE expansion of the partition function, at least in zero-dimensions (i.e. the simple integral of $\exp\{-x^2 - \lambda x^4\}$ for x from $-\infty$ to $+\infty$).

Note the absence of a 1D case in table 1. This is because the method does not produce any critical points in the 1D case, which is physically correct — there are no phase transitions in the 1D Ising model. We have already alluded to quantitative similarities between our model and mean field theory. The fact that we do not find a phase transition in the 1D case is a step better than mean field theory, which does predict a phase transition in the 1D Ising model.

Finally, we also used MAPLE to check the critical behaviour in the Ising model. Using the expressions for three dimensions we were able to show that the critical exponent δ is indeed precisely 3.

Order	κ_c for 2D		
1	$1/4$		
2	$4/12 =$	$1/3 =$	.3333333333
3	$12/(104/3) =$	$9/26 =$	.3461538462
4	$(104/3)/92 =$	$26/69 =$	.3768115942
5	$92/(3608/15) =$	$345/902 =$	.3824833703
6	$(3608/15)/(9148/15) =$	$902/2287 =$	.3944031482
7	$(9148/15)/(485788/315) =$	$48027/121447 =$	.3954564543
	κ_c for 3D		
1	$1/6$		
2	$6/30 =$	$1/5 =$	.2000000000
3	$30/148 =$	$15/74 =$	.2027027027
4	$148/706 =$	$74/353 =$	.2096317280
5	$706/(16804/5) =$	$1765/8402 =$	.2100690312
6	$(16804/5)/15746 =$	$8402/39365 =$	.2134383335
7	$15746/(7742666/105) =$	$826665/3871333 =$	.2135349762
	κ_c for 4D		
1	$1/8$		
2	$8/56 =$	$1/7 =$	.1428571429
3	$56/(1168/3) =$	$21/146 =$	.1438356164
4	$(1168/3)/(7976/3) =$	$146/997 =$	.1464393180
5	$(7976/3)/(272176/15) =$	$4985/34022 =$	.1465228382
6	$(272176/15)/(614728/5) =$	$34022/230523 =$	.1475861411
7	$(614728/5)/(262409816/315) =$	$4840983/32801227 =$	.1475854242
	κ_c for d		
1	$1/(2d)$		
2	$(2d)/(4d^2-2d) =$	$1/(2d-1)$	
3	$(4d^2-2d)/(8d^3-8d^2+4d/3(?))$		

Table 5: Exact critical points for the 2D, 3D and 4D Ising models The values are obtained by using the linear variational parameter j only. For 3D the Monte Carlo result is $\kappa_c = 0.221654$ [49, 72, 73].

5 Conclusions

We have studied the LDE together with several different optimisation schemes for the Ising, model, spin-one model and full $\lambda\phi^4$ field theory. In doing so we have gone four orders higher than any previous LDE lattice study except for the pure gauge study of Kerler and Metz [19]. In any case, to the best of our knowledge, the Ising and spin-one models have not previously been studied on the lattice using LDE. To reach our high orders we had to automate the whole diagrammatic expansion procedure. While similar expansions (high-temperature etc.) have been done to much higher orders elsewhere (e.g. see [57, 58]), these non-LDE studies do not have the optimisation stage of the LDE method. This means the limitations in terms of computing are quite different for LDE, we must calculate the whole expression for the free energy many many more times and our expressions have several extra parameters. Thus we have achieved one of our aims which was to demonstrate that high orders of LDE lattice expansions can be calculated without using significant computing resources. In doing so we have indicated some of the

key issues and our solutions to several problems.

It is clear to us that the method could be improved in several places and higher orders reached, e.g. through the use of the 'free diagrammatic expansion' [77]. Though we could never match the orders produced for straight high-temperature expansions, experience with LDE in QM has been that the variational aspect more than compensates for the additional work or in our case, low numbers of terms in our expansions.

We studied several different optimisation schemes, PMS (Principle of Minimal Sensitivity) and FAC (Fastest Apparent Convergence) but in this particular case, only our use of the minimum free energy principle seemed to work. It is hard to find detailed comparisons of optimisation schemes or to find the use of the minimal free energy condition in the literature of LDE on the lattice, so it is hoped that our results have moved the debate on.

We also note that all our work, and that of the LDE lattice literature, is exclusively on a simple cubic lattice, though of various dimensions. It would be straightforward to repeat our calculations for other lattices, just as high temperature expansions have been done. We merely note that calculations up to third order on a hypertetrahedral lattice have shown the expected variation in the position of critical points but there is no sign of a change in the critical exponents.

We set out to use the calculation of critical exponents as a test of the LDE method, at least for this lattice approximation. As such we have shown that the LDE method has failed to capture the non-perturbative infra-red physics of scalar filed models near the critical point as all our results have given the incorrect mean field values. This is despite us pushing the calculation to far higher orders and studying the region close to the transition extremely carefully, taking great care to keep numerical errors under control. The fact that low orders produce these mean field values is not too surprising, as the exact analysis of the Ising model demonstrates, but we are unable to explain why the LDE method does not start to move towards the correct values as we study higher orders. In most studies where exact results are known (typically quantum mechanics) moving to higher and higher orders in the LDE method rapidly brings one to good approximations of non-perturbative results. Our conclusion is that this form of LDE on the lattice is unable to access the non-perturbative aspects of field theories near the critical point.

This is not necessarily the end of the use of LDE for field theories. We are studying a theory which is not-asymptotically free, using a space-time lattice and only looking at one type of physics. LDE calculations for QCD, using continuous space-time methods[13] or even for other quantities might show better results. One might try to find a different way of applying the LDE in this case. After all, the high-temperature expansion gives a series which itself necessarily has *no* transitions yet by using Padé methods and similar one can extract remarkably good results. Such methods are not directly applicable to LDE as it does *not* calculate coefficients of a series. LDE only provides a sequence of results which in some testable cases converge extremely fast to the correct answer. For the LDE the most obvious variation is to try different ansatz for the trial action S_0. We have indicated that it must be ultra-local for calculational reasons, but beyond that we have great flexibility. For instance we tried ansatz such as

$$L_0 = j\phi + k\phi^2 + q|\phi|^p + l\phi^4 \tag{82}$$

with non-polynomial power p a variational parameter. However our studies at low orders

[13]We note, however, that that the results of Gandhi and McKane [30] for critical exponents using LDE with continuum space-time methods were only slightly better. See also the work of Ogure and Sato [31, 35], and Chiku [32].

showed no promise and we did not pursue this further.

Acknowledgements

We would like to acknowledge S.Hands, H.F.Jones, R.J.Rivers and A.Ritz for many useful comments. TSE would like to thank K.George, R.Johnson, K.Kiyani, C.Mukherjee, R.Richardson and V.Stojevic for their contributions to the preliminary investigations of these models.

References

[1] I.Montvay and G.Münster, "Quantum Fields on a Lattice", Cambridge University Press, 1994.

[2] J.Zinn-Justin, "Quantum Field Theory and Critical Phenomena", (Oxford University Press, Oxford, 1996, 3rd edition).

[3] A.Duncan and M.Moshe, "Nonperturbative physics from interpolating actions", Phys.Lett. **215** (1988) 352.

[4] H.F.Jones, Nucl.Phys.B (Proc.Suppl.) **39** (1995) 220.

[5] C.M.Bender et al., "Logarithmic Approximations to Polynomial Lagrangeans", Phys. Rev. Lett. **58** (1987) 2615.

[6] C.M.Bender et al., "Novel perturbative scheme in quantum field theory", Phys. Rev. D **37** (1988) 1472.

[7] C.M.Bender and H.F.Jones, "New nonperturbative calculation: Renormalization and the triviality of $(\lambda\phi^4)_4$ field theory", Phys. Rev. D **38** (1988) 2526.

[8] C.M. Bender and H.F. Jones, "Evaluation of Feynman diagrams in the logarithmic approach to quantum field theory", J. Math. Phys. **29** (1988) 2659.

[9] P.M.Stevenson, "Optimised Perturbation Theory", Phys.Rev.**D23** (1981) 2916.

[10] S.Chiku and T.Hatsuda, "Optimised perturbation Theory at Finite Temperature", PRD **58** (1998) 076001 [hep-ph/9803226].

[11] P.M.Stevenson, "Gaussian Effective Potential: Quantum Mechanics", Phys.Rev.D **30** (1984) 1712.

[12] A.N.Sissakian, I.L.Solovtsov and O.P.Solovtsova, Phys.Lett.B **321** (1994) 381.

[13] H.Kleinert, Phys.Lett.**A173** (1993) 332.

[14] W.Janke and H.Kleinert, Phys.Rev.Lett.**75** (1995) 2787.

[15] H.Kleinert and V.Schulte-Frohlinde, "Critical Properties of ϕ^4-Theories" (World Scientific, Singapore, 2001).

[16] F. Karsch, A. Patkós and P. Petreczky, "Screened Perturbation Theory", Phys.Lett.B **401** (1997) 69 [hep-ph/9702376].

[17] V.I.Yukalov, J.Math.Phys. **33** (1992) 3994.

[18] C.M.Wu et al., "Phase Structure of Lattice ϕ^4 Theory by Variational Cumulant Expansion", Phys.Lett.B **216** (1989) 381.

[19] W. Kerler and T. Metz, "High-order effects in action-variational approaches to lattice gauge theory", Phys.Rev.D **44** (1991) 1263.

[20] I.R.C. Buckley, A. Duncan and H.F. Jones, "Proof of the convergence of the linear δ expansion: Zero dimensions", Phys.Rev.D **47** (1993) 2554.

[21] C.M.Bender, A.Duncan and H.F.Jones, Phys.Rev.D **49** (1994) 4219.

[22] A.Okopińska, "Nonstandard expansion techniques for the effective potential in $\phi^4(x)$ quantum field theory", Phys.Rev**D35** (1987) 1835.

[23] S.A. Pernice and G. Oleaga, "Divergence of perturbation theory: Steps towards a convergent series", Phys. Rev. D **57** (1998) 1144.

[24] C.M.Bender, K.A.Milton, S.S.Pinsky and L.M.Simmons Jr., J.Math.Phys. **30** (1989) 1447.

[25] W.E.Caswell, Ann.Phys. **123** (1979) 153.

[26] J.Killingbeck, J.Phys.A **14** (1981) 1005.

[27] A.Duncan and H.F.Jones, "Convergence proof for optimised δ expansion: Anharmonic oscillator", Phys.Rev.D **47** (1993) 2560.

[28] R.Guida, K.Konishi and H.Suzuki, Ann.Phys. **249** (1996) 106.

[29] A. Okopińska, "Nonstandard expansion techniques for the finite-temperature effective potential in $\lambda\phi^4$ quantum field theory", Phys. Rev. D **36** (1987) 2415.

[30] S.K.Gandhi and A.J.McKane, "Critical Exponents in the δ-expansion", Nucl.Phys.B **419** (1994) 424

[31] K. Ogure and J. Sato, "Critical exponents and critical amplitude ratio of the scalar model from finite-temperature field theory", Phys. Rev. D **57**, 7460 (1998) [arXiv:hep-ph/9801439].

[32] S.Chiku, "Optimised perturbation Theory at Finite Temperature - two-loop analysis", Prog.Th.Phys **104** (2000) 1129, hep-ph/0012322

[33] Y.Meurice, "A Simple Method to Make Asymptotic Series of Feynman Diagrams Converge", Phys.Rev.Lett. 88 (2002) 141601.

[34] E.Braaten and E.Radescu, "Convergence of the Linear δ expansion in the Critical $O(N)$ Field Theory", Phys.Rev.Lett. **89** (2002) 271602.

[35] K. Ogure and J. Sato, "Critical exponents of O(N) scalar model at temperatures below the critical value using auxiliary mass method", Prog. Theor. Phys. **102**, 209 (1999) [hep-ph/9905370].

[36] T.S. Evans, H.F. Jones and D. Winder, "Non-perturbative calculations of a global $U(2)$ theory at finite density and temperature", Nucl. Phys. B **598** (2001) 578.

[37] J.O.Akeyo and H.F.Jones, Phys.Rev.D **47** (1993) 1668.

[38] J.O.Akeyo and H.F.Jones, Z.Phys.C **58** (1993) 629.

[39] J.O.Akeyo, H.F.Jones and C.S.Parker, "Extended Variational Approach to the SU(2) Mass Gap on the Lattice", Phys.Rev.D **51** (1995) 1298.

[40] X.-T.Zheng, Z.G.Tan and J.Wang, Nucl.Phys.B **287** (1987) 171.

[41] J.M.Yang, J.Phys.G **17** (1991) L143.

[42] J.M.Yang, C.M.Wu and P.Y.Zhao, J.Phys.G **18** (1992) L1.

[43] X.-T.Zheng, B.S.Liu, Intl.J.Mod.Phys.A **6** (1991) 103.

[44] C.-I. Tan and X.-T. Zheng, "Variational-cumulant expansion in lattice gauge theory at finite temperature", Phys. Rev. D **39** (1989) 623.

[45] T.S. Evans, M. Ivin and M. Möbius, "An optimised perturbation expansion for a global O(2) theory", Nucl. Phys. B **577** (2000) 325.

[46] D. Winder, "Investigating Phase Transitions using the Linear Delta Expansion", Ph.D. Thesis, Imperial College, University of London, UK, 2001.

[47] T.S.Evans, H.F.Jones and A.Ritz, "An Analytical Approach to Lattice Gauge-Higgs Models", in "Strong and Electroweak Matter '97", ed. F.Csikor and Z.Fodor (World Scientific, Singapore, 1998).

[48] T.S.Evans, H.F.Jones and A.Ritz, "On the Phase Structure of the 3D SU(2)-Higgs Model and the Electroweak Phase Transition", Nucl.Phys. **B517** (1998) 599.

[49] M. Hasenbusch, K. Pinn and S. Vinti, "Critical Exponents of the 3D Ising Universality Class From Finite Size Scaling With Standard and Improved Actions", `arXiv:hep-lat/9806012`.

[50] H.W.J. Blöte, E. Luijten and J.R. Heringa, "Ising universality in three dimensions: a Monte Carlo study", J. Phys. A **28** (1995) 6289.

[51] S.-J.Chang, "Quantum fluctuations in a ϕ^4 theory. I. Stability of the vacuum", Phys. Rev. D **12** (1975) 1071.

[52] I.G.Halliday and P.Suranyi, "Anharmonic oscillator: A new approach", Phys. Rev. D **21** (1980) 1529.

[53] M.Wortis, "Linked Cluster Expansion", in "Phase Transitions and Critical Phenomena", vol.3, eds. C.Domb and M.S.Green (Academic Press, London, 1974).

[54] F.Englert, "Linked Cluster Expansions in the Statistical Theory of Ferromagnetism", Phys. Rev. **129** (1963) 567.

[55] G.S. Rushbrooke, "On the Theory of Randmly Dilute Ising and Heisenberg Ferromagnets", J. Math. Phys. **5** (1964) 1106.

[56] G.S. Rushbrooke, G.A. Baker, Jr. and P.J. Wood, in "Phase Transitions and Critical Phenomena", Volume 3, edited by C. Domb and M.S. Green (Academic Press, 1974).

[57] H.Meyer-Ortmanns and T.Reisz, Nucl.Phys.B (Proc.Suppl.) **73** (1999) 892.

[58] M.Campostrini et al., "Critical behaviour of the three-dimensional XY universality class", Phys.Rev.B **63** (2001) 214503.

[59] B. Bollobás, "Modern Graph Theory" (Springer, 1998).

[60] R. Brout, "Statistical Mechanical Theory of a Random Ferromagnetic System", Phys. Rev. **115** (1959) 824;

[61] R.Brout, "Statistical Mechanical Theory of Ferromagnetism. High Density Behavior", Phys. Rev. **118** (1960) 1009;

[62] R.Brout, "Statistical Mechanics of Ferromagnetism; Spherical Model as High-Density Limit", Phys. Rev. **122** (1961) 469.

[63] G. Horwitz and H.B. Callen, "Diagrammatic Expansion for the Ising Model with Arbitrary Spin and Range of Interaction", Phys. Rev. **124** (1961) 1757.

[64] B. Strieb, H.B. Callen and G. Horwitz, "Cluster Expansion for the Heisenberg Ferromagnet", Phys. Rev. **130** (1963) 1798.

[65] S. Sherman, "Product Property and Cluster Property Equivalence", J. Math. Phys. **5** (1964) 1137.

[66] D.Stauffer and A.Aharony, "Introduction to Percolation Theory" (Taylor and Francis, 1994).

[67] S.Mertens, "Lattice Animals: A Fast Enumeration Algorithm and New Perimeter Polynomials", J.Stat.Phys. **58** (1990) 1095

[68] B.D.McKay, *nauty*, `http://cs.anu.edu.au/~bdm/nauty/`

[69] Waterloo Maple, `http://www.maplesoft.com/`

[70] W.H.Press, S.A.Teukolsky, W.T.Wetterling and B.P.Flannery, "Numerical Recipes in C++", (Cambridge University Press, Second Edition,2002).

[71] GNU Multiple Precision Library, `http://www.swox.com/gmp`

[72] A.M.Ferrenberg and D.P.Landau, "Critical behavior of the three-dimensional Ising model: A high-resolution Monte Carlo study", Phys.Rev.B**44** (1991) 5081.

[73] A.L. Talapov and H.W.J. Blöte, "The magnetization of the 3D Ising model", J. Phys. A **29** (1996) 5727.

[74] K. Hagiwara et al., "The Review of Particle Physics", Physical Review D**66**, 010001 (2002)

[75] K. Huang, E. Manousakis and J. Polonyi, "Effective potential in scalar field theory",, Phys. Rev. D **35** (1987) 3187.

[76] J. Kuti and Y. Shen, "Supercomputing the Effective Action", Phys. Rev. Lett. **60** (1988) 85.

[77] C.Itzykson and J.-M.Drouffe, "Statistical Field Theory, vol 2" (Cambridge University Press, Cambridge, 1989).

[78] Mathematica, `http://www.wolfram.com/`

[79] S. Chiku, "Optimised Perturbation Theory at Finite Temperature — Two-Loop Analysis —", Prog. Theor. Phys. **104** (2000) 1129.

A Growing unique configurations

For diagrams of n links (an abstract graph), we could easily construct all possible configurations (embeddings of this graph on a space-time lattice) by throwing down n links in all possible ways on all the lattice graph edges in an $(n+1)^d$ size box, but every configuration then appears in $(n+1)^d$ copies differing only by translation invariance. This is clearly highly inefficient at the orders and dimensions we work at so the aim of the algorithm outlined here is to produce a complete set of configurations of a certain size, once and only once, modulo translation symmetry. The algorithm is inspired by those described for percolation simulations [66, 67].

The starting point is to define some relation on the edges in the configurations, so that we can always decide that any certain line is 'greater' or 'less' than any other line. To do this, we first have to define a relation on the points of the lattice, and so we say that a point $\boldsymbol{x} = (x_1, x_2, \ldots, x_d)$ is *greater* than a point $\boldsymbol{y}$, i.e. $\boldsymbol{x} > \boldsymbol{y}$, if the first coordinate of $\boldsymbol{x}$ is greater than the first coordinate of $\boldsymbol{y}$, $x_1 > y_1$. If the two coordinates happen to be equal, then we compare the second coordinates in the same way. If these turn out to be equal, we continue moving on to the next coordinate until we have exhausted all the d coordinates that label a point on the lattice.

$$\boldsymbol{x} > \boldsymbol{y} \Leftrightarrow \exists\, i \text{ s.t. } x_i > y_i \text{ and } x_j = y_j \;\forall\; j < i, \quad i, j \in \{1, 2, \ldots, d\} \tag{83}$$

Of course, if all the coordinates turn out to be the same, the two points p_1 and p_2 are equal.

In our configurations edges, have no directions but it is always useful to list them with the least vertex first. An edge is then an ordered pair of two (neighbouring) points $\mathsf{e} = (\boldsymbol{x}, \boldsymbol{x}_{\rm nn}), \boldsymbol{x} < \boldsymbol{x}_{\rm nn}$. To define a relation between two edges e and f, we say that e is *greater* than f if e's first vertex is greater than the first vertex of f. If the two points happen to be equal, then we compare the second coordinate in the same way.

$$\mathsf{e} > \mathsf{f} \Leftrightarrow \exists\, i \text{ s.t. } e_i > f_j \text{ and } e_j = f_j \;\forall\; j < i, \quad i, j \in \{1, 2\} \tag{84}$$

The relation we defined on the lines will ensure that *every configuration* has a *unique least* line. This link goes through the least vertex of the configuration which we choose to be the origin $\mathcal{O}$ on the space-time lattice. All the configurations we create have the origin as the least vertex as then we are guaranteed that all our configurations are not related by translation symmetry to any of the others we produce.

What then remains to be done is to ensure that we grow *all possible* configurations *once and only once* from this lowest vertex origin. A recursive algorithm which does this is as follows. For an existing configuration of n links, C_n, the set of possible lines to be added is an ordered list of links, $\mathcal{L}_n$, in which each link satisfies the following five conditions:

1. they never contains a vertex less than the origin $\mathcal{O}$ (eliminates translations),

2. they start from an existing vertex in the configuration (we are not interested in disconnected graphs),

3. they do not lie on top of any other links (we are not interested in non-simple graphs),

4. they are always greater than the least link in the existing configuration C_n (ensures we visit each configuration only once, and none are related by translation invariance as the first and least line remains the least line)

5. each link has not been investigated at previous orders even if it is not in the existing configuration C_n (ensures each configuration is visited once and only once)

We then add a link to C_n, starting with the least link in the list of possible links $\mathcal{L}_n$, creating a configuration C_{n+1} of $n+1$ links. We then recurse, considering possible links to add to this $n+1$ link configuration, C_{n+1}. We stop recursing when R links have been added. Once we have considered adding one link to the n-link configuration, say $e_i \in \mathcal{L}_n$, and all the possible larger configurations coming from that, before we consider the next possible link, $e_{i+1} \in \mathcal{L}_n$ for this n-link configuration C_n, we mark the link just investigated, e_i, in the lattice as having been *used*. This enables the implementation of the fifth condition in the production of the lists $\mathcal{L}_m$ $(m > n)$ and is vital to eliminate repetitions of the same configuration.

Note we do not generate configurations in the order of their links. The relation (84) gives a natural order for the links in every configuration but many configurations have links which are connected to each other only via links which are greater than both of them. This is why the fourth condition only requires potential new links to be greater than the first one.

To see how this works, or to test the voracity of alternative algorithms, the example of $d = 2$ space-time dimensions on a square lattice up to configurations of $R = 3$ links is often sufficient. For instance consider the two size 2 configurations of figure 15. With the first coordinate up the page, the second to the right of the origin $\mathcal{O}$, we exclude the lattice vertices shown as open circles by rule one and so eliminate repetitions related by space-time translation. It also follows that configuration (a) is generated before configuration (b) so this is why the link labelled X has can not be used in the latter, by rule five. Without this limitation, the order 3 configuration using link 4 in case (a) would have been reproduced by case (b) with link X since the latter link is legitimate by all the other rules.

B Free Energy Density

The calculation of the free energy density is based on the formalism developed in section 2 with the free energy density given as an expansion of order R

$$f^{(R)} = -\sum_{n=0}^{R} \frac{\delta_2^n}{n!} f_{1n} = -\sum_{n=0}^{R} \frac{\delta^n}{n!} f_n \tag{85}$$

We also know that $f_0 = \ln \mathcal{Z}_0$, and for the other f_n's, we have to make use of all the different connected graphs of size n and their multiplicities. For $n = 1$ this is a particularly easy task, but the $n = 2$ term is illustrative, yet simple enough to work through as an example.

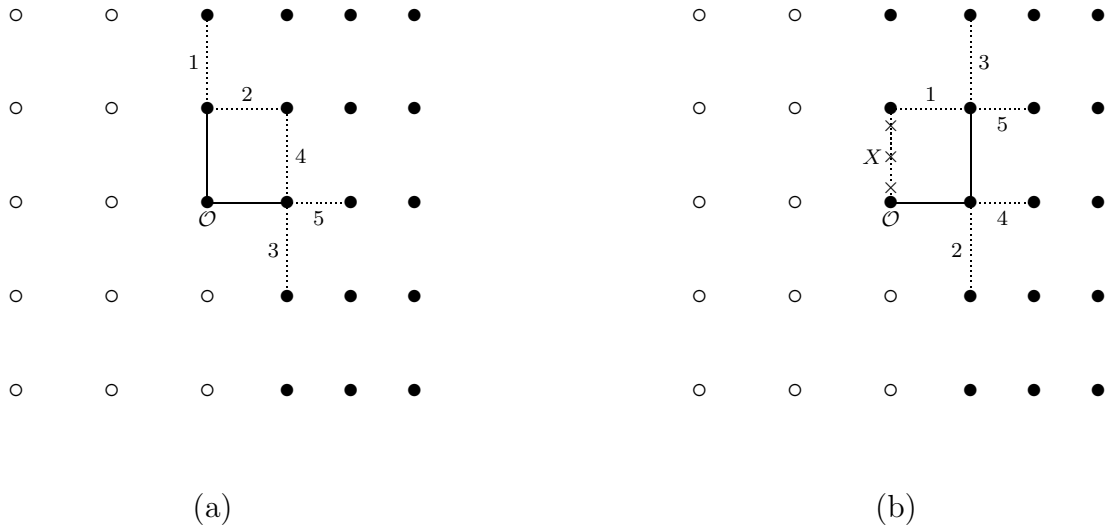

(a) (b)

Figure 15: Two different second order configurations are shown in solid lines. The first coordinate is measured up from the origin $\mathcal{O}$, the second coordinate is measured to the right of the origin. Thus the vertex points with open circles are never used to ensure that the origin $\mathcal{O}$ is always the smallest vertex, thus eliminating space-time translations of diagrams. The links which can be added to produce third order diagrams are given as dashed lines, numbering reflecting the edge ordering as defined in the text, i.e. $e_i < e_j$ if $i < j$. Edge X in case (b) is crossed out to indicate it is excluded by our rule five ensuring that when link 4 is added to configuration (a), the resulting order 3 configuration is not produced from configuration (b).

The diagram counting is the first step in the numerical evaluation of any f_n. The `C/C++` program implementing the algorithm for counting multigraphs without loops is used to find the multiplicities of all the graphs of size 2 and less. Note that the multiplicities will depend on the dimension of the problem, i.e. the dimension of the lattice that the configurations are generated on. For definiteness we will consider the example of a $d = 3$ cubic lattice. The program will output the results in a text file, and for our example we get

$$3 \quad \bullet\!\!-\!\!\bullet \qquad\qquad 3 \quad \bullet\!\!=\!\!\bullet \qquad\qquad 30 \quad \bullet\!\!-\!\!\bullet\!\!-\!\!\bullet \tag{86}$$

The numbers preceding the graphs are the multiplicities, the number of distinct ways these graphs can be embedded on a space-time lattice up to translations. Thus f_{11}, f_{22} are

$$f_{11} = 3\langle \bullet\!\!-\!\!\bullet \rangle_{\rm C} \tag{87}$$

$$f_{12} = 30\langle \bullet\!\!-\!\!\bullet\!\!-\!\!\bullet \rangle_{\rm C} + 3\langle \bullet\!\!=\!\!\bullet \rangle_{\rm C} \tag{88}$$

The cumulant expectation values then have to be expanded in terms of statistical averages using equation (38). For example,

$$\langle \bullet\!\!-\!\!\bullet\!\!-\!\!\bullet \rangle_{\rm C} = \langle \bullet\!\!-\!\!\bullet\!\!-\!\!\bullet \rangle_1 - \langle \bullet\!\!-\!\!\bullet \rangle_1 \langle \bullet\!\!-\!\!\bullet \rangle_1 \tag{89}$$

These graphs can be in terms of fields, physical and variational parameters, and the expectation values with respect to the L_1 trial Lagrangian fields at one site. Using (30) these last contributions are expressed in terms of the J_p integrals of (31). For instance

$$\langle \bullet\!\!-\!\!\bullet\!\!-\!\!\bullet \rangle_1 = \frac{J_1}{J_0}\frac{J_1}{J_0} \tag{90}$$

However, the J_n integrals contain δ_1 in their exponents through L_1. Terms such as f_{12} are already order $(\delta_2)^2$ so they can have their J_n integrals simply replaced by I_n of (15). However f_{11} have only one power of delta so they require us to expand the J_n integrals to first order in δ_1 and the terms from $f_{10} = \ln(J_0)$ require full second order expansions. For the Ising model case we have

$$J_n := I_n + \delta_2 \Delta J I_{n+1} + \frac{1}{2}(\delta_2 \Delta J)^2 I_{n+2} + O((\delta_2)^3) \tag{91}$$

where $\Delta J = J - j$. Inserting into (87) truncating at order of delta $R = 2$ and then setting the δ's equal to one, we finally get the following expression for second order term of the full free energy, f_2:

$$\begin{aligned} f_2 \;=\; & 30\left[\langle\phi\rangle_0^2\langle\phi^2\rangle_0 - \langle\phi\rangle_0^4\right] + 3\left[\langle\phi^2\rangle_0^2 - \langle\phi\rangle_0^4\right] \\ & +12\Big[\langle\phi\rangle_0\left[(j-J)\langle\phi^2\rangle_0 + (k-\alpha)\langle\phi^3\rangle_0 + (l-g)\langle\phi^5\rangle_0\right] \\ & -\langle\phi\rangle_0^2\left[(j-J)\langle\phi\rangle_0 + (k-\alpha)\langle\phi^2\rangle_0 + (l-g)\langle\phi^4\rangle_0\right]\Big] \\ & +(j-J)^2\langle\phi^2\rangle_0 + (k-\alpha)^2\langle\phi^4\rangle_0 + (l-g)^2\langle\phi^8\rangle_0 \\ & +2\left[(j-J)(k-\alpha)\langle\phi^3\rangle_0 + (j-J)(l-g)\langle\phi^5\rangle_0 + (k-\alpha)(l-g)\langle\phi^6\rangle_0\right] \\ & -(j-J)^2\langle\phi\rangle_0^2 - (k-\alpha)^2\langle\phi^2\rangle_0^2 - (l-g)^2\langle\phi^4\rangle_0^2 \\ & -2\big[(j-J)(k-\alpha)\langle\phi\rangle_0\langle\phi^2\rangle_0 + (j-J)(l-g)\langle\phi\rangle_0\langle\phi^4\rangle_0 \\ & +(k-\alpha)(l-g)\langle\phi^2\rangle_0\langle\phi^4\rangle_0\big] \end{aligned} \tag{92}$$

where $\langle\phi^p\rangle_0 = I_p/I_0$.

We have shown the above expression in its entirety to demonstrate the general form of the f_n. Thus we see that the calculation of f_n is broken down into a sum of terms (the number of which will get rather large as we go to higher orders) depending on the physical parameters J, α and g, the variational parameters j, k and l, and also the field expectation values $\langle\phi^p\rangle_0$. Note that the $\langle\phi^p\rangle_0$ actually depend *only* on the variational parameters. From a numerical perspective, however, we look upon the $\langle\phi^p\rangle_0$ as quantities in their own right since their evaluation is a non-trivial task. Thus, mathematically we write $f^{(R)}(J, \alpha, g; j, k, l)$ to indicate the variables which contribute to the calculation of $f^{(R)}$. On the other hand, numerically we recognise that in order to calculate $f^{(R)}$, we also need to address separately the calculation of a set of $\langle\phi^p\rangle_0$'s.

Maple is the ideal tool to perform all the necessary expansions, starting from the appropriate list of diagrams and multiplicities such as (86), through to obtaining the expressions for the f_n. For the particular case of $n = 2$, this will be an expression of the form shown in equation (92) above. Maple will output f_2 as code in the `C` programming language, optimising the sum for minimum computation. We note that this output was always checked up to 3rd order against code that we had available from the study of a complex ϕ^4 theory [45]. By performing this 3rd order check routinely, we gained confidence in the validity of our diagram counting and code generating techniques.

C Numerical Accuracy

The standard double precision available to `C/C++` (type `double`) is limited to around 17 decimal places of precision on floating point numbers.[14] The nature of the calculations

[14]Technically, this will depend on the computer architecture and the particular C/C++ implementation. We used a standard PC based on an AMD Athlon XP 2100+ processor (a 32-bit architecture), and

in our model is such that there are many additions and subtractions, with a very wide range of values. Here we have to deal with the common problem of terms in a summation conspiring to cancel out in such a way that smaller terms fail to contribute to a sum in which their contribution is, in fact, important. This is the *rounding* problem.

C.1 Free Energy Density

Now consider an example from our actual model — the calculation of $f^{(R)}$ for a set of physical and variational parameters. The numerical values of the parameters in this example are taken from one of the points visited by the program as it searches for the critical point. This is a realistic scenario for the double precision program, since it is taken at a stage where the program is exploring variations of the order of 10^{-15} in the free energy. This is the sort of accuracy we would expect to achieve from an implementation using `C/C++`'s standard double precision. The values of interest are listed in table 6.

f_n	Smallest	Largest	Total
$n = 1$	$1.4997840002 \cdot 10^{-10}$	$2.7472168610 \cdot 10^{-10}$	$-9.1453475295 \cdot 10^{-11}$
$n = 2$	$4.6741039631 \cdot 10^{-22}$	$7.4509483795 \cdot 10^{-2}$	$-7.4509483756 \cdot 10^{-2}$
$n = 3$	$2.0210522783 \cdot 10^{-29}$	$7.4509483795 \cdot 10^{-2}$	$-6.4570642135 \cdot 10^{-11}$

Table 6: The table summarises the absolute values of the smallest and largest terms in the sums which constitute the f_n terms, for all orders up to the third. The total value of each order is given too. These particular values are taken from a real calculation of $f^{(R)}$ close to the critical point.

The third order proves already to be numerically both interesting and challenging. The smallest term being of the order of 10^{-29} and the largest of 10^{-2}. The total result is of the order of 10^{-11}, and is arrived at by summing 93 terms[15] whose values will range from the smallest to the largest quoted in the table. It is obvious that if we are limited to double precision floating point arithmetic, we could easily end up completely losing contributions from terms that might actually be important, especially, one suspects, near physical transition points. One could argue that since the largest term is of the order of 10^{-2} and the total is about 10^{-11}, we are actually only in danger of losing approximately 9 decimal places in this case, which should still be well covered by the 17 decimal places that double precision offers.

However it is not the free energy itself but differences in the free energies for similar parameter values which we are interested in, as we are trying to find a set of variational parameters which minimise the free energy. For instance, the values discussed above are derived from a point which is used to calculate differences in free energies of size 10^{-15} only. Requiring greater accuracy of the free energy would require calculations involving even smaller values of the variational parameters, which also means a greater range of values appearing in the terms that contribute to the f_n.

Even if this level of accuracy is acceptable for this 3rd order case that we are presenting, higher orders will further increase the disparity of the terms. For all these reasons we decided to use an arbitrary precision package, the GNU Multiple Precision (GMP) [71] library. GMP fixes a number of bits which are allocated to the mantissa of a floating point number. This means that by setting the precision of the mantissa to, for example,

we used Linux with the GNU Compiler Collection v3.2 implementation of C/C++.

[15] In the 4D case.

128 bits, the largest number we can accurately represent is approximately $2^{128} \approx 3.4 \cdot 10^{38}$. In other words, we will have approximately 38 decimal places of accuracy. When we discuss the results we will find numerous occasions where we really use the extra precision made available to us by the GMP library. For instance, we were able to minimise the free energy density to one part in 10^{-40}.

C.2 Integration

It has been emphasised that the calculation of the free energy density (and for that matter, any other quantity with the LDE formalism) will depend in particular on field expectation values at a single site taken with respect to the trial action $\mathcal{S}_0$ which depends on the variational parameters j, k and l, and of the form

$$\mathcal{S}_0(j,k,l) = j\phi + k\phi^2 + l\phi^4 \tag{93}$$

We introduced in (15) the notation I_p for the general form of the relevant integrals

$$I_p = \int_{-\infty}^{+\infty} \mathrm{d}\phi\, \phi^p \exp\left[-j\phi - k\phi^2 - l\phi^4\right] \tag{94}$$

These are trivial for the Ising and spin-one models but non-trivial for the full ϕ^4 model. This is the case we consider in this section.

Being quartic in the exponential, the calculation of the I_p's is a necessary numerical consideration. Numerical integration comes with its own set of problems though. For small j, the most interesting case for transitions, and for p odd, the integrand is nearly odd so to avoid severe rounding problems we used the half-range integral forms

$$I_p = 2\int_0^{+\infty} \mathrm{d}\phi\, \phi^p \cosh(j\phi)\, e^{-k\phi^2 - l\phi^4} \qquad \text{for } p \text{ even} \tag{95}$$

$$I_p = 2\int_0^{+\infty} \mathrm{d}\phi\, \phi^p \sinh(-j\phi)\, e^{-k\phi^2 - l\phi^4} \qquad \text{for } p \text{ odd} \tag{96}$$

Having reduced the I_p's to integrals over half the real line, we have (approximately) halved the number of interpolations that need to be performed in order to numerically evaluate the integrals. This will be an obvious computing time bonus, but we have also given ourselves a break from the dangerous 'rounding-off' error that appears in sums when terms are of opposite signs.

Another important issue is the infinite range of integration. Our integrand is suppressed at large ϕ by the negative terms in the exponential. We will typically have $l = 25$, and, for example, if we were to introduce the cutoff for the upper limit at $\phi = 3$, the exponential would look like $\exp\{-3j - 9k - 2025\}$. Thus the variational parameters j and k would have to be significantly large negative numbers to create a dent in the assumption that this exponential is vanishingly small, and in practice they are of the same order of magnitude as the corresponding physical parameters and so $O(10)$ at most. So it is easy to find a suitable cutoff value for ϕ in the I_p integrals. The numerical tests discussed below make it clear that we can indeed trust our numerical integration.

Note that for *every single* evaluation of the free energy in the ϕ^4 model, which will depend on the physical parameters as well as the variational parameters, we will have to evaluate a *complete* set of I_p's, from $p = 0$ through to whatever the upper limit on p turns out to be. For example, in a 3rd order expansion we are looking at the range

$0 \leq p \leq 12$, the upper limit coming from a term in which the quartic ϕ^4 from the exponential is cubed upon expansion. For a 7th order expansion this range will thus go up to 28. We used a standard Romberg integration method, with additional polynomial extrapolation of successive refinements to zero stepsize [70]. However we adapted this to perform the integration of all the required I_p's in parallel. Thus, instead of working with a single integrand (corresponding to a specific value of p), we manipulate a whole vector of elements, one entry for the integrand at each value of p required.

The integrals and the numerical methods used to calculate them are not unusual. However, we did require much higher accuracy than normal so we will note how we tested our integration. For the purpose of testing, we used the following values for the variational parameters:[16]

$$j = 8.16343354579642367932991357923 \cdot 10^{-10} \tag{97a}$$
$$k = -7.6 - 1.58180882338368170019383733935 \cdot 10^{-9} \tag{97b}$$
$$l = 25 \tag{97c}$$

Using 256 bit floating point arithmetic, approximately 77 decimal places of precision, table 7 shows a comparison of our results for the above integrals for various values of p with the best results we could get for the same integral calculated using numerical integration in Mathematica [78].

p	I_p
0	1.67769083077124890028663394770701193593 1.67769083077124890028663394770701193592521428271904249117805060996740
1	$1.81907694824780353539804027376 \cdot 10^{-10}$ $1.81907694824780353539804027376452421473264747834415743104674406673865 \cdot 10^{-10}$
6	0.014383378315767397063832614328941243024492875427108307844390698790 0.014383378315767397063832614328941243024492875427108307844390698790
11	$5.60612966361923040128191595587443818807152405548720830361149104778581 \cdot 10^{-13}$ $5.60612966361923040128191595587443818807152405548720830361149104778581 \cdot 10^{-13}$
12	0.000686736730588807286984362186205281300199335600989584639188353746380 0.000686736730588807286984362186205281300199335600989584639188353746380

Table 7: The table shows results of evaluating the integrals I_p for various p, with the variational parameters as given in (97). For each value of p we show the result from Mathematica (first row), and the result from our integration routine (second row). Our results are calculated with 256 bit floating point arithmetic; we show approximately 70 decimal places (we expect the results to be that accurate).

A slightly different check was performed on the I_0 integral for $j = k = 0$ and $l = 1$ and $l = 25$, which is simply $2\Gamma(5/4)(l)^{-1/4}$. Mathematica has no problem evaluating the Gamma function to very high precision. We found that our integration routine matched the 150 decimal places of Mathematica's results.[17]

[16] The apparent randomness of the values is due to the fact that these constituted a point of contention in the early stages of development of the program; it subsequently assumed a status of a testing point.

[17] To achieve this accuracy we used 512 bit floating point arithmetic.

Arithmetic / Tolerance	κ_c
64 bit / 10^{-10}	0.2027041103
64 bit / 10^{-15}	0.202702704077629
128 bit / 10^{-10}	0.2027041103
128 bit / 10^{-15}	0.202702704077255
128 bit / 10^{-20}	0.20270270272418008017
128 bit / 10^{-25}	0.2027027027027865987084316
128 bit / 10^{-30}	0.202702702702702784632396012135
256 bit / 10^{-20}	0.20270270272418008017
256 bit / 10^{-25}	0.2027027027027865987084316
256 bit / 10^{-30}	0.202702702702702784632395797442
256 bit / 10^{-35}	0.20270270270270270302274056635402966
256 bit / 10^{-40}	0.202702702702702702703952850607590698 5909

Table 8: The table summarises the critical inverse temperatures κ_c found for the 3D Ising model at 3rd order. Each row represents a run with a different precision on the internal arithmetic and tolerance value for the simplex optimisation. The values of κ_c are given to as many decimal places as is allowed by the tolerance required on the minimum of $f^{(3)}$.

D Benefits of High Precision Arithmetic

Many studies based on LDE compatible methods (e.g. [30, 31, 35, 79]) noted the similarity between their critical exponents and those obtained by mean field theory. Indeed, in preparing the results for [45], we also noticed that critical exponents calculated with our 3rd order LDE method produce values equivalent to mean field theory results. For this reason, one of the main goals of this study was to estimate critical exponents with high numerical accuracy, in particular to establish any possible deviations from the mean field results as higher orders of the LDE are considered.

As a prerequisite, we must find the critical point. Table 8 summarises the estimates of κ_c for the 3D Ising model at 3rd order. The values were found by searching for the value of κ where $\left\langle \bar{\phi} \right\rangle^{(3)}(\kappa, J = 0)$ switches between zero and non-zero values. We will now explain the significance of the results given in the table.

The results are all obtained with an implementation using the GNU multiple precision library (GMP). The first two rows show results obtained using 64 bits of precision, which is comparable to the built-in double precision arithmetic of `C/C++`. The remaining rows were calculated with significantly higher precision. 128 bit arithmetic gives us approximately 38 digits of precision, while for 256 bit arithmetic we get approximately 77 digits. Every row is also labelled by a certain tolerance, which is the termination criterion for the simplex minimisation routine.

To understand what the numbers are telling us, we have to explain the route by which they are obtained. The quantity which is minimised to the tolerance setting is the third-order free energy density $f^{(3)}$ of the free energy. The I_p's are evaluated to high accuracy since they are simple functions in the Ising model. Once evaluated, these are combined with the physical and variational parameters to form $f^{(R)}$. The minimisation routine keeps the physical parameters (κ and J) constant, but varies the variational parameters (only j in this case) until it hits a minimum in $f^{(R)}$. The procedure will continue minimisation until it is satisfied that it has reached the tolerance which is required of it. That is

why we quote κ_c in table 8 with as many decimal places as the free energy was minimised to.

Although $f^{(R)}$ is minimised to within some quoted tolerance of the minimum point, there is *no reason to assume* that the variational parameters have been fixed to the same accuracy. In fact, experience shows that relatively large variations in the variational parameters (of the order of ϵ, say) produce relatively small variations in $f^{(R)}$ (of the order of ϵ^2). This should come as no surprise, because we expect linear variations not to contribute at a stationary point. Moreover, this lends support to the reasoning of the PMS criterion, since it is our goal to fix the variational parameters in a way which will leave the physics as independent of the variational parameters as possible.

For this simple Ising model case the exact location of the critical point is $15/74 \approx 0.2027027027\ldots$ (see section 4.2). We see in table 8 that the numerical accuracy in κ_c increases as we increase the tolerance as long as this is paired with enough accuracy provided by the internal arithmetic. If we require a tolerance of 10^{-40} on the free energy, we are confident that j is correct to within approximately 10^{-20} of its value. This explains why the values of κ_c in table 8 follow the exact result up to about half of the decimal places displayed.